Study of Low-Temperature Effects in Silicon-Germanium Heterojunction Bipolar Transistor Technology

A Thesis
Presented to
The Academic Faculty

by

Adnan Ahmed

In Partial Fulfillment
of the Requirements for the Degree
Master of Science
in School of Electrical and Computer Engineering

Georgia Institute of Technology
August 2005

Study of Low-Temperature Effects in Silicon-Germanium Heterojunction Bipolar Transistor Technology

Approved by:

Professor John D. Cressler, Advisor
School of Electrical and Computer Engineering
Georgia Institute of Technology

Professor Joy Laskar
School of Electrical and Computer Engineering
Georgia Institute of Technology

Professor John Papapolymerou
School of Electrical and Computer Engineering
Georgia Institute of Technology

Date Approved: May 6, 2005

ACKNOWLEDGEMENTS

First and foremost, I am grateful to God Almighty for the blessings He has bestowed upon me. I am thankful to my family, whose continuous encouragement, unconditional love, and support has been the source of motivation for me all throughout my life. I would especially like to express my gratitude towards my parents, Dr. Syeda Farida Begum, and Dr. Aftab Uddin Ahmed, for all their sacrifice, and for always being there for me.

I am truly indebted to my graduate advisor, Dr. John D. Cressler, for his guidance, leadership, support, and patience, throughout my master's program. I am thankful to the members of my thesis advisory committee, Dr. John Papapolymerou, and Dr. Joy Laskar, for their time, and advice. I would like to acknowledge that this work would not have been possible without the help of my fellow lab mates and colleagues in the Silicon Germanium Devices and Circuits Group, at the Georgia Institute of Technology, Atlanta, Georgia. I am grateful to Aravind Appaswamy, Akil Sutton, Curtis Grens, Tianbing Chen, and Ramkumar Krithivasan, for assisting me during the data gathering and analysis phases of this work.

Finally, I would like to acknowledge Alvin Joseph, and the IBM SiGe team for providing the hardware for this study, and NASA for financially supporting this project.

TABLE OF CONTENTS

ACKNOWLEDGEMENTS . . . . . **iii**

LIST OF TABLES . . . . . **vi**

LIST OF FIGURES . . . . . **vii**

SUMMARY . . . . . **x**

I INTRODUCTION **1**

1.1 Motivation 1

1.2 SiGe HBT BiCMOS Technology 3

1.2.1 SiGe Strained Layer 4

1.2.2 Fabrication Techniques 5

1.2.3 Technology Generation and Scaling 7

1.3 Device Physics of SiGe HBTs 11

1.4 Second Order Effects 16

1.4.1 Ge-grading Effect 16

1.4.2 Tunneling Effect 17

1.4.3 Heterojunction Barrier Effect 18

1.5 Breakdown Fundamentals 21

1.6 Summary 24

II CRYOGENIC OPERATION OF SIGE HBTS **25**

2.1 Introduction 25

2.2 Background 25

2.3 Static Characteristics of First Generation SiGe HBTs 29

2.3.1 Experimental Setup 29

2.3.2 High Performance Results and Discussion 29

2.3.3 High Breakdown Results and Discussion 41

2.3.4 Profile Design and Optimization 51

2.4 Summary 51

III IMPLICATIONS OF TECHNOLOGY SCALING ON CRYOGENIC STATIC PERFORMANCE OF SIGE HBTS 53

3.1 Introduction 53

3.2 Background 54

3.2.1 Description of Technology 54

3.2.2 Experimental Setup 54

3.3 Results and Discussion 55

3.3.1 Second Generation SiGe HBT Static Characteristics 55

3.3.2 Third Generation SiGe HBT Static Characteristics 59

3.3.3 Fourth Generation SiGe HBT Static Characteristics 62

3.3.4 Summary 69

IV CONCLUSION 70

4.1 Conclusion 70

4.2 Future Directions 71

REFERENCES 72

LIST OF TABLES

1 Characteristic device parameters for four SiGe BiCMOS technology generations (after [20], [21], [22], [23]). 8

LIST OF FIGURES

1 2-D schematic representation of both strained and relaxed SiGe on a Si substrate, [3]. 4

2 SiGe strained layer thermodynamic stability diagram. Dotted lines represents Matthews and Blakeslee theoretical result, [3]. 6

3 Schematic cross-section of an UHV/CVD reactor, [6]. 7

4 Vertical SIMS profile showing doping concentration and Ge profile within a first generation SiGe HBT. 9

5 A schematic device cross-section of a third generation BiCMOS SiGe HBT. . . 10

6 Energy band diagram for a graded base SiGe HBT and a Si BJT. 12

7 Representative Gummel plot for a SiGe HBT as compared to a Si BJT. 14

8 The Late Effect, [32]. 17

9 2-D schematic of the tunneling process, [10]. 19

10 Cutoff frequency as a function of collector current density for three generations of SiGe HBT BiCMOS technology. 22

11 Schematic illustration of the avalanche multiplication process in a reversed bias p-n junction. 23

12 Forced I_E method for M-1 calculation, [10]. 24

13 Gummel characteristic for a first generation SiGe at different temperatures. . . 26

14 Biasing conditions for the Gummel and Output Characteristics. 30

15 HP4155. 30

16 Gummel Characteristic of IBM 5AM HP at different temperatures. 31

17 Current Gain for IBM 5AM HP at different temperatures. 32

18 Slope of Gummel Characteristic vs. Collector Current Density for IBM 5AM HP at T=300K. 33

19 Slope of Gummel Characteristic vs. Collector Current Density for IBM 5AM HP at T=162K. 33

20 Slope of Gummel Characteristic vs. Collector Current Density for IBM 5AM HP at T=43K. 34

21 Slope of Gummel for IBM AM HP at 162K under a collector-emitter bias of 1V. 34

22 Forced V_{BE} Output Characteristic of IBM 5AM HP at T=300K. 36
23 Forced V_{BE} Output Characteristic of IBM 5AM HP at T=43K. 37
24 Early Voltage Extraction. 37
25 Variation of Early Voltage, V_A, with temperature for IBM 5AM HP. 38
26 Variation of Avalanche Factor, M-1, with temperature for IBM 5AM HP. 39
27 Variation of BV_{CEO} with temperature for IBM 5AM HP. 39
28 Forced I_B Output Characteristic of IBM 5AM HP at high injection at T=300K. 40
29 Forced I_B Output Characteristic of IBM 5AM HP at high injection at T=162K. 40
30 Forced I_B Output Characteristic of IBM 5AM HP at high injection at T=43K. . 41
31 Gummel Characteristic of IBM 5AM HB at different temperatures. 42
32 Current Gain for IBM 5AM HB at different temperatures. 42
33 Comparison of Gummel Characteristics of IBM 5AM HP and HB at different temperatures. 43
34 Comparison of Current Gains for IBM 5AM HP and HB at different temperatures. 44
35 Slope of Gummel Characteristic vs. Collector Current Density for IBM 5AM HB at 150K. 44
36 Slope of Gummel Characteristic vs. Collector Current Density for IBM 5AM HB at 162K. 45
37 Slope of Gummel Characteristic vs. Collector Current Density for IBM 5AM HB at 43K. 45
38 Forced V_{BE} Output Characteristics for IBM 5HB at 300K. 47
39 Forced V_{BE} Output Characteristics for IBM 5HB at 93K. 48
40 Variation of Early Voltage with temperature for IBM 5AM HB Technology. . . 48
41 Variation of BV_{CEO} with temperature for IBM 5AM HB Technology. 49
42 Forced I_B Output Characteristics for IBM 5AM HB at 300K. 49
43 Forced I_B Output Characteristics for IBM 5AM HB at 162K. 50
44 Forced I_B Output Characteristics for IBM 5AM HB at 43K. 50
45 Gummel Characteristic of IBM 7HP at different temperatures. 55
46 Current Gain for IBM 7HP at different temperatures. 56

47 Slope of Gummel Characteristic vs. Collector Current Density for IBM 7HP at 300K. 57

48 Slope of Gummel Characteristic vs. Collector Current Density for IBM 7HP at 150K. 57

49 Slope of Gummel Characteristic vs. Collector Current Density for IBM 7HP at 50K. 58

50 Gummel Characteristic for IBM 8HP at different temperatures. 59

51 Current Gain for IBM 8HP at different temperatures. 60

52 Slope of Gummel Characteristic vs. Collector Current Density for IBM 8HP at 300K. 60

53 Slope of Gummel Characteristic vs. Collector Current Density for IBM 8HP at 150K. 61

54 Slope of Gummel Characteristic vs. Collector Current Density for IBM 8HP at 50K. 61

55 Forward Mode Collector Current Density for IBM 9HB at different temperatures. 63

56 Forward Mode Base Current Density for IBM 9HB at different temperatures. . 63

57 Current Gain for IBM 9HB at different temperatures. 64

58 Slope of Gummel Characteristic vs. Collector Current Density for IBM 9HB at 300K. 64

59 Slope of Gummel Characteristic vs. Collector Current Density for IBM 9HB at 150K. 65

60 Slope of Gummel Characteristic vs. Collector Current Density for IBM 9HB at 50K. 65

61 Gummel Characteristic for all four technology generations at 300K and 43K. . 67

62 Current Gain for all four technology generations over temperature. 67

63 Peak Current Gain for all four technology generations over temperature. 68

SUMMARY

This thesis investigates the low-temperature effects of Silicon Germanium (SiGe) Heterojunction Bipolar Transistors (HBT) BiCMOS technology. A comprehensive set of *dc* measurements were taken on first, second, third and fourth generation IBM SiGe HBT BiCMOS technology over a range of temperatures (room temperature to 43K for first generation, and room temperature to 15K for the rest).

In Chapter I, important background information, such as the history, fabrication, device physics, and expected performance of SiGe HBT devices are discussed. In Chapter II, theory behind the cryogenic operation of SiGe HBTs is presented, followed by the description of the experimental procedures and extraction techniques used to reach the results, and finally the results are presented and discussed. Results for two flavors, High Performance and High Breakdown of first generation technology are then compared.

Chapter III focuses on discussing and comparing variation of static performances with temperature. for all the four technology generations of SiGe HBT devices. Chapter IV concludes the thesis and mentions what future work can be done to further our knowledge in this area.

This work is unique in the sense that this sort of comprehensive study of dc characteristics on all commercially available SiGe HBT BiCMOS technology generations over a wide range of temperatures has never been done before to the best of the author's knowledge

CHAPTER I

INTRODUCTION

1.1 Motivation

The wireless communication marketplace has grown enormously over the past decade. The deployment of first generation analog and second generation digital cellular systems like GSM, PHS, iDEN enjoyed great success and changed the wireless communications market's primary focus from professional to consumer. It has been estimated that by the year 2010, the number of wireless subscribers will reach one billion and exceed the number of wireline subscribers [1]. The Technology Industry Association mentions in their 2005 Telecommunications Market Review and forecast that the total revenue in 2004 for the wireless communications market was 2.1 trillion, which was 9.4% higher from 2003, and was projected to grow for the period 2004-2008 [2].

With the advent of the Information Age, companies need to differentiate their products and to satisfy the appetite of the consumer in the future, more features and services must be provided. To accommodate and accelerate the growth of subscriber units of ever increasing complexity and capability in the future, cost effective and power efficient multi-band, multi-mode transceivers will be required. In addition, new uses for data, particularly at higher data rates such as required for the transmission of high frame rate video will likely drive many future applications. These new applications place new requirements on technology, and new challenges for technologists [1].

In today's multi-functional cell phones, the individual functional blocks are made with specialized IC technologies and are packaged separately, which allows a cost effective implementation. For example, GaAs MESFET/HBT may be used in the Low Noise Amplifier (LNA) and Power Amplifier (PA), Si BJT may be used in the mixer, oscillator,

and converter, while Si CMOS technology may be used in the baseband processing and digital signal processing unit (DSP) [3]. But, given the demanding market trends and consumer wants, it is becoming increasingly necessary to reduce form factor, cost, simultaneously with improving performance. For this, revolutionary solutions such as System-on-a-Package (SOP) are necessary. However, in the long run, for ultimate integration, System-on-a-Chip (SOC) is the solution. This would allow to achieve reduced form factor, longer battery life, reduced packaging complexity, and ultimately lower total system cost. This however would require the whole system to be built using one common technology, which has to combine the superior RF and analog performance properties of III-V technology with Si CMOS for digital and memory functions, all married together with Si IC manufacturing, in other words, a Si-compatible III-V technology! [3]. This technology exists, and Silicon-Germanium HBT technology is it. It's time has come!

A small but important niche market for SiGe HBT technology is in cryogenic electronics, with applications such as high sensitivity cooled sensors and detectors, superconductor hybrid systems space-born electronics and cryogenically cooled computer systems. Traditionally, cryogenic studies of transistors have been used chiefly as a tool to understand the device physics behind them, but the clear advantages of SiGe HBTs over Si BJT, as was documented theoretically and experimentally in [4] and [5], has made it a subject of interest. It is true that since it is a bipolar technology, there is a large power dissipation associated with it, and will preclude its use in widespread cooling constrained cryogenic systems. However, its ease of integration with low-power, scaled, CMOS in SiGe HBT BiCMOS technology overrides that disadvantage. Furthermore, cryogenic applications aside, most electronics which have to meet military specifications, need to operate over a temperature range of -55 to 125 degrees Celsius, and those that need to meet commercial specifications, need to operate within 0 to 85 degrees Celsius. Therefore, understanding the behavior of SiGe HBT BiCMOS technology at low temperature is crucial if it is to enable the next generation of commercial electronics of the Information Age.

The primary goal of this thesis is to investigate the transistor level static performance implications of cryogenic operation of SiGe HBT BiCMOS technology. We will try to achieve this goal by presenting and analyzing the *dc* characterization results of various generations of SiGe HBT BiCMOS devices taken over a range of temperatures.

1.2 SiGe HBT BiCMOS Technology

"What is claimed is:

1) ...

2) A device as set forth in claim 1 in which one of the separated zones is one of a semiconductive material having a wider energy bandgap than that of the material in other zones.

Claim 2 of U.S. Patent 2 569 347 to W. Schockley,

Filed 26 June 1948

Issued 25 September 1951

Expired 24 September 1968" [7]

As can be seen above, the idea of making a heterojunction transistor is as old as the transistor itself, but unfortunately, its revival was possible only in the early 1970's when the technology to build these transistors, Molecular Beam Epitaxy (MBE) [8] and Metal Oxide Chemical Vapor Deposition (MOCVD) [9], came into being. And it was not until the 1990's, until the advent of Ultra High Vacuum/Chemical Vapor Deposition (UHV/CVD), that SiGe HBTs were produced in a large-scale. This is ironic as the first functional transistor was made using Ge. Ge actually has better electron mobility, $\mu_{n,Ge}$=3500 cm^2/V-sec, than Si, $\mu_{n,Ge}$=3500 cm^2/V-sec, at 300K for N_{AD}=10^{6}cm^{-3} [10]. However, it is not as cheap to manufacture and as abundant as Si. A brief history of SiGe HBT technology can be found in [3]. The first functional SiGe HBT was demonstrated in December 1987 [11].

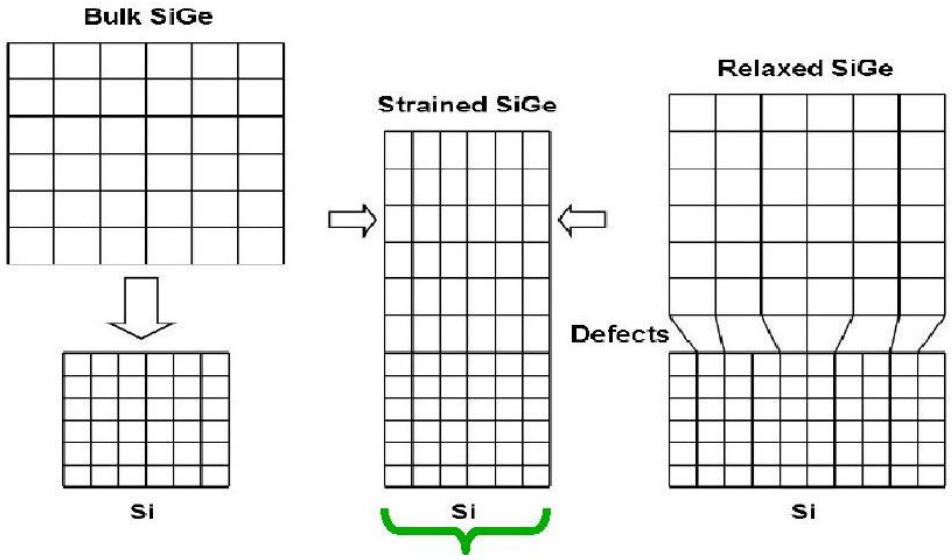

Figure 1: 2-D schematic representation of both strained and relaxed SiGe on a Si substrate, [3].

1.2.1 SiGe Strained Layer

Si and Ge are both Group IV elemental semiconductors and are completely miscible over their entire compositional range. The lattice structure of SiGe alloy has a diamond structure and has a linearly interpolated constant given by Vegard's rule:

$$a(Si_{1-x}Ge_x) = a_{Si} + x(a_{Ge} - a_{Si}) \tag{1}$$

Where a is lattice constant and x is Ge fraction.

SiGe alloy is deposited epitaxially over a thick Si substrate, the buffer layer, and is sandwiched by another Si layer deposited on top of it, the cap layer. The inherent lattice mismatch between the two materials is accommodated either by the SiGe film adapting to its host's smaller lattice constant (pseudomorph) or by "relaxing" during growth to its natural lattice constant. Relaxation introduces many defects, which are detrimental to the operation of the device, so the growth is preferred [11]. Pseudomorphically formed SiGe films become 'metastable' after certain thicknesses are reached, h_{crit}, which depends on the Ge content, x, in the film, as shown by Matthews and Blakeslee in [12] and [13], and

can spontaneously relax under thermal processing. Equation 2 captures the relationship between x and h_{crit}.

$$x = \frac{bcos\lambda}{0.084h_{crit}} \left\{ \gamma + \frac{1-\nu/4}{4\pi cos^2\lambda cos\phi(1+\nu)} \left\{ (ln\frac{h_{crit}+H}{b} + \delta ln\frac{H}{b} - \delta ln\frac{1}{y} \right\} \right\} \quad (2)$$

where b is magnitude of Burger's vector, λ is angle between b and interface normal to dislocation line, ϕ is angle between slip plane and normal vectors to the strained interface, ν is the parametric constant, and δ and γ are given by $\delta = \frac{H}{h_{crit}+H}$ and $\gamma = \frac{h_{crit}}{h_{crit}+H}$.

For a position dependent Ge profile, the stability point must be calculated as an average value of Ge fraction across h according to

$$\bar{x} = \frac{1}{h}\int_0^h x(z)dz \quad (3)$$

The ordered pair [$\bar{x}$,h] can then be placed on a stability diagram, Figure 2, and compared to the theoretical calculation of h_{crit} cs $\bar{x}$ for various values of Si cap layer thickness, H.

1.2.2 Fabrication Techniques

The fabrication of a SiGe HBT is identical to that of a Si BJT except for the addition of Ge into the base region. The epitaxial growth of the SiGe pseudomorphic layers require the balancing of two competing temperature dependent requirements, namely, mobility of the adhering atomic species and formation of dislocation nucleation. As for increased mobility, large temperatures are preferred, but to avoid strain relaxation by enhanced dislocation formation, low temperatures are necessary. Fundamental growth studies, [14], have shown 550 degrees Celsius to be optimal for good quality epitaxial growth for moderate Ge concentrations (<15%).

The growth of SiGe epitaxial films has been attempted by various techniques, including MBE, [15] and [16], limited Reaction Processing (LRP) or Rapid thermal Chemical Vapor Deposition (RTCVD) [17], Atmospherice Pressure Chemical Vapor Deposition (APCVD) [18], and UHV/CVD [19]. UHV/CVD is the best among them for large-scale integration and batch production. It eliminates the high thermal budget of conventional epitaxy by

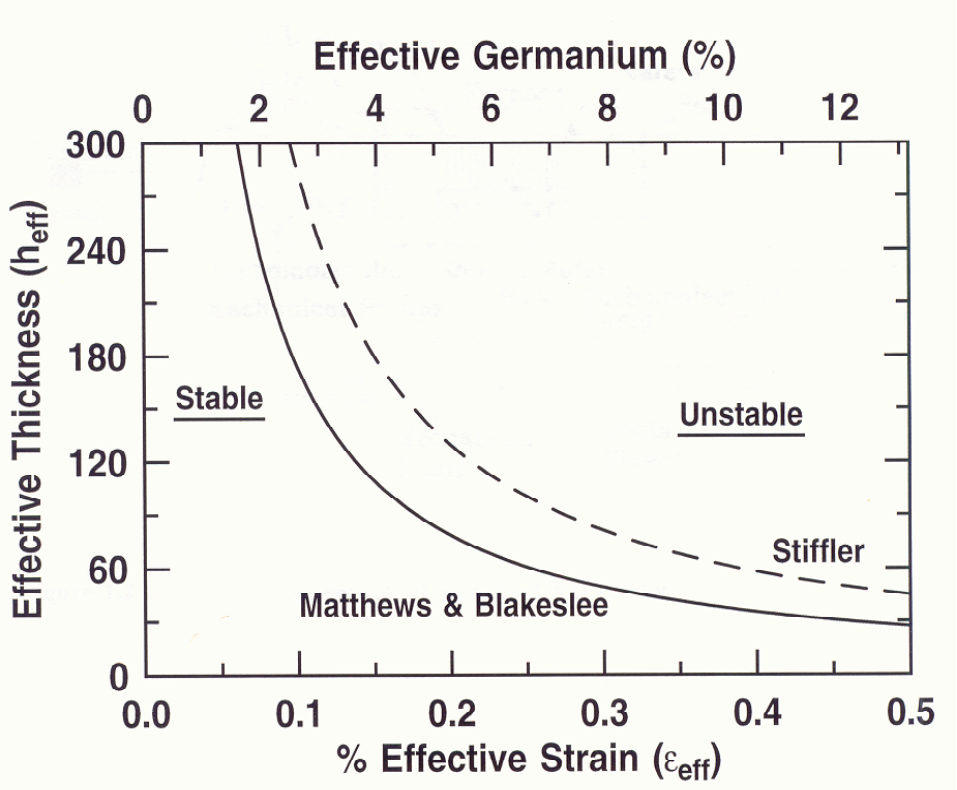

Figure 2: SiGe strained layer thermodynamic stability diagram. Dotted lines represents Matthews and Blakeslee theoretical result, [3].

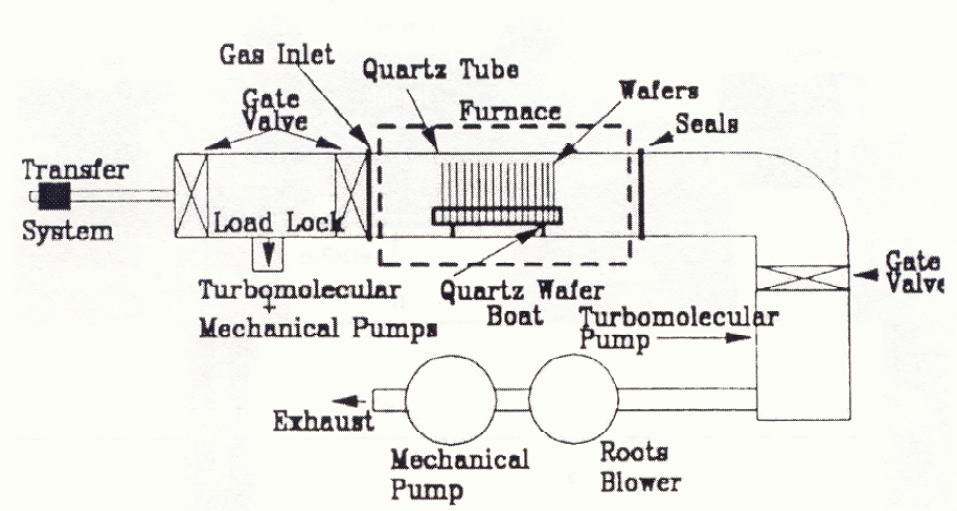

Figure 3: Schematic cross-section of an UHV/CVD reactor, [6].

chemical means. Films are deposited by UHV/CVD at temperature ranges of 400-500 degrees Celsius, those temperatures corresponding to the growth of pure Ge, and pure Si, respectively [3]. It is operated at a vacuum of 10^{-6}torr. Gaseous sources employed are silane (SiH_4), germane (GeH_4), diborane (B_2H_6), and phosphine (PH_3). Film growth rates vary with Ge content but typical rates are 4-40 Angstroms/minute [3]. See Figure 3 to see a cross-section of a UHV/CVD system.

1.2.3 Technology Generation and Scaling

The goal of this section is to introduce the various SiGe HBT BiCMOS technologies in production currently. The discussion will be limited to only self-aligned, fully integrated, Si-processing compatible HBT technologies manufactured by IBM. IBM was chosen, out of the 40 odd foundries all over the world which are manufacturing SiGe, as they were the first to commercialize the technology and have four generations of the technology currently in production.

The four generations of technology and their typical static and dynamic performances can be seen in Table 1. The compatibility of SiGe HBT technology with state-of-the-art Si CMOS technology is very important in SiGe HBT BiCMOS. For IBM 5HP, the respective

Table 1: Characteristic device parameters for four SiGe BiCMOS technology generations (after [20], [21], [22], [23]).

Parameter	IBM 5HP	IBM 7HP	IBM 8HP	IBM 9T
$W_{E,eff}$ (μm)	0.5	0.2	0.12	0.12
peak β	100	200	400	650
V_A (V)	65	120	> 150	>150
BV_{CEO} (V)	3.3	2.5	1.7	1.7
BV_{CBO} (V)	10.5	7.5	5.5	5.6
peak f_T (GHz)	48	120	207	300
peak f_{max} (GHz)	69	100	285	350
min. NF_{min} (dB)	0.8	0.4	< 0.3	-

CMOS has an effective length of 0.35 μm with 3.3V V_{DD} [25]. For IBM 7HP, it has 0.18 μm (1.8V V_{DD}) and 0.3 μm (3.3V V_{DD}) Si CMOS devices [26]. For IBM 8HP, two types of 130 nm Si CMOS devices are available, with minimum channel lengths of 0.12 μm (1.2V V_{DD}) and 0.24 μm (2.5V V_{DD}).

The fabrication steps for a first generation SiGe HBT (IBM 5HP) technology starts with an n+ subcollector (5-10Ω/sq) on a p- substrate (10^{-15}Ω-cm) while a lightly doped n-type collector (0.4-0.6μm at 5x10^{15}cm^{-3}) is used as collector. A composite SiGe epilayer, consisting of a Si buffer (10-20nm), boron-containing (1-3x10^{13}cm^{-3}) SiGe/SiGeC layer (70-100nm thick), and a Si cap layer (10-30nm thick) form the base. The polysilicon emitter is heavily doped with As up to the solid solubility limit, by implantation, or in-situ. It is fully self-aligned to the base using Emitter-Base (EB) spacers. Silicided extrinsic base and selectively implanted collectors (SIC reachthroughs, 10-20Ωμ^2) are used to reach the base and the sub-collector. The resulting HBT has a metallurgical base width of about 90nm (65nm neutral base width under forward-active bias), metallurgical emitter junction depth of about 35nm, and a peak Ge content of 8%. The peak boron doping is around 4x10^{18}cm$^-$3. (R_{bi}=6kΩ/sq approx.). A typical SIMS profile for IBM 5HP can be seen in Figure 4.

The second (IBM 7HP) and third (IBM 8HP) generations are scaled versions of the

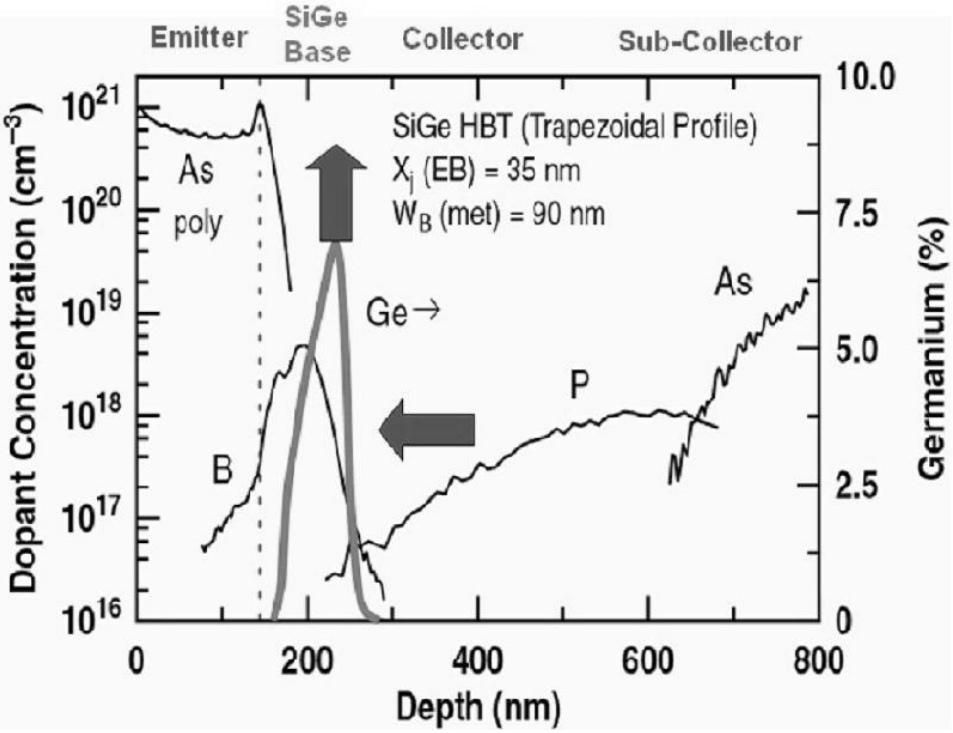

Figure 4: Vertical SIMS profile showing doping concentration and Ge profile within a first generation SiGe HBT.

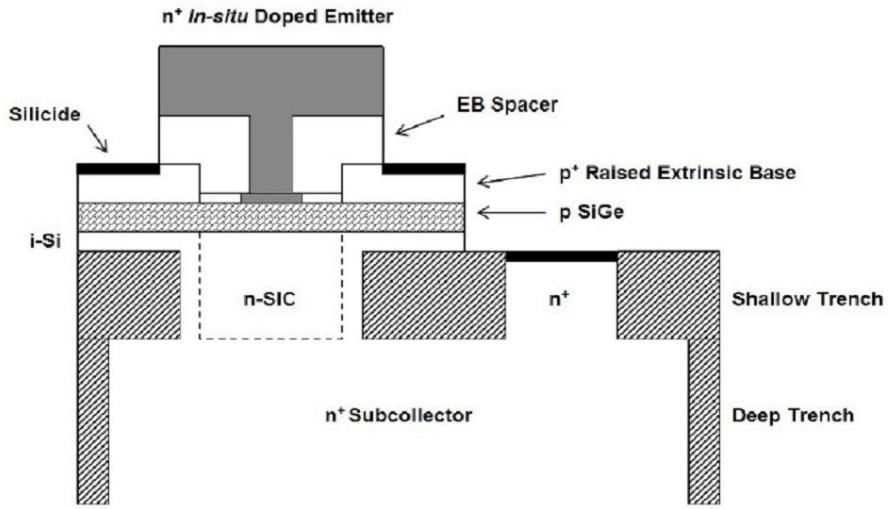

Figure 5: A schematic device cross-section of a third generation BiCMOS SiGe HBT.

first. IBM 7HP was laterally and vertically scaled to achieve W_E=0.2μm. Thinner base means reduced parasitics, higher peak Ge content, and larger resistances, which is compensated with higher base doping. These factors result in reduced carrier transit time, and thus higher device performance. The low thermal budget of UHV/CVD is necessary to maintain the thinness of the base region due to the diffusive nature of boron in Si [22].

The 3rd generation uses a new NPN structure, with a raised extrinsic base using conventional deep and shallow trench isolation (STI) to achieve simultaneously high f_T and f_{max} dynamic performance. The vertical and lateral dimensions were reduced compared to IBM 7HP. The collector and base doping were raised. The Ge content was raised to a thermodynamically stable 25%, and the SiGe film was grown using conventional non-selective UHV/CVD batch processing [22]. A representative cross-section of the device can be seen in Figure 5.

The 4th generation achieved a record high peak-f_T of 350GHz and emitter-to-collector transit time (τ_{EC}) of 0.45ps, for any Si-based transistor, with a 67% peak-f_T rise of peak over the previous performance record [23]. The BV_{CEO} and BV_{CBO} were 1.7 and 5.6V respectively, and the Johnson's limit, ($f_T.BV_{CEO}$) [27], was well above 200GHz and the f_{max}

for IBM 9T is also above 300GHz [24]. The cross-section of an IBM 9T device resembles that of IBM 8HP, except for the aggressive vertical scaling, and carefully optimized adjustments made to the Ge profile, base width (W_B), and dopant profiles, that made the improvements possible.

It is important to mention that each IBM technology generation usually comes in two flavors, "high performance", and "high breakdown". Since there is a fundamental tradeoff between current gain and breakdown voltage for SiGe HBTs, these two flavors are offered to circuit designers for use in different circumstances. The high breakdown device is typically a high performance device with lower collector doping, which effectively increases its BV_{CEO}, but also allows high injection effects to occur at lower injections and reduce current gain prematurely. This tradeoff will be discussed in more detail in later sections.

1.3 Device Physics of SiGe HBTs

The bandgap of Ge is 0.66eV and Si is 1.12eV at 300K. Therefore the bandgap of the SiGe base is less than that of the Si emitter and collector and is tunable (approx. -7.5meV per 1% Ge). The result of this dissimilar bandgaps are a band offsets caused by the presence of Ge at the Emitter-Base (EB) and the Collector-Base (CB) junctions of the transistor, $[\Delta E_{g,Ge}(x = 0)]$ and $[\Delta E_{g,Ge}(x = W_b)]$, respectively. Also, depending on the Ge profile shape, there may be a Ge grading across the base, $[\Delta E_{g,Ge}(x = 0)]$. These three factors and their effect on the energy band diagram of the SiGe HBT can be seen in Figure 6. The figure overlays the band diagram of both the SiGe HBT and a standard Si BJT biased in forward active mode.

The effect of $[\Delta E_{g,Ge}(x = 0)]$ on the band diagram translates to a lower barrier for minority carriers to enter the base from the emitter and the effect of $[\Delta E_{g,Ge}(x = 0)]$, is to allow the carriers to travel by a predominantly drift over diffusion mechanism. This increases collector current density (J_C) for the same biasing conditions, i.e. base-emitter voltage (V_{BE}), base current density (J_B), as a standard Si BJT. Therefore, the current gain

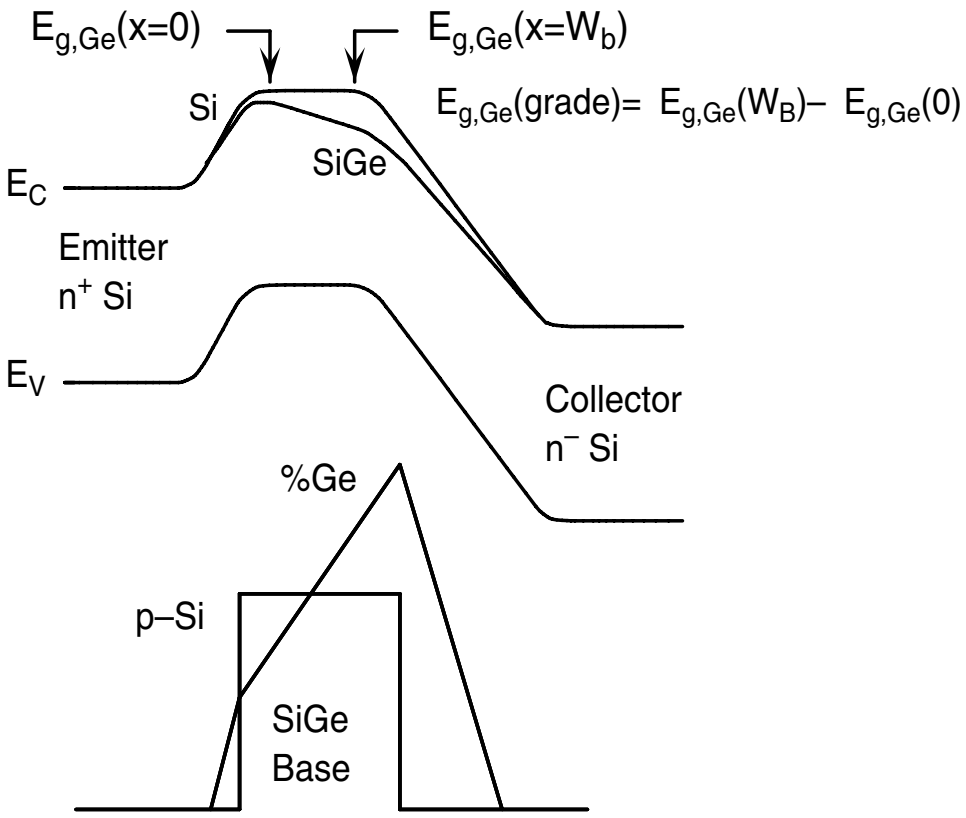

Figure 6: Energy band diagram for a graded base SiGe HBT and a Si BJT.

for a SiGe HBT is higher than its Si counterpart. The inherent compressive strain build-up in the pseudomorphically formed SiGe base, due to the lattice mismatch between Si and SiGe, enhances the mobility of carriers, and effectively accentuates this advantage of SiGe HBT.

The expression for J_C can be obtained using the Moll-Ross relation [28].

$$J_C = \frac{q(e^{qV_{BE}/kT-1})}{\int_0^{W_b} \frac{p_b(x)dx}{D_{nb}(x)n_{ib}^2(x)}} \tag{4}$$

J_C depends on the bandgap offsets through the intrinsic carrier density, n_{ib}^2 and carrier diffusivity, D_{nb} functions.

$$n_{ib}^2 = \gamma n_{io}^2 e^{\Delta E_{gb}^{app}/kT} e^{[\Delta E_{g,Ge}(grade)]x/(W_b kT)} e^{\Delta E_{g,Ge}(0)/kT} \tag{5}$$

The low-doping intrinsic carrier density for Si is $n_{io}^2 = N_C N_V e^{-E_{go}/kT}$, $\gamma = (N_C N_V)_{SiGe}/(N_C N_V)_{Si} < 1$ is the effective density-of-states ratio between SiGe and Si [29], and ΔE_{gb}^{app} is the apparent bandgap narrowing resulting from heavy doping in the base.

Assuming a linearly graded Ge profile ($\Delta E_{g,Ge}(grade) = \Delta E_{g,Ge}(W_b) - \Delta E_{g,Ge}(0)$), from Equations (4) and (5), an overall expression for collector current density (J_C) in a SiGe HBT can be reached [30],[31].

$$J_{C,SiGe} = \frac{qD_{nb}}{N_{ab}^- W_b}\left(e^{qV_{BE}/kT} - 1\right) n_{io}^2 e^{\Delta E_{gb}^{app}/kT}\left\{\frac{\widetilde{\gamma}\widetilde{\eta} e^{\Delta E_{g,Ge}(0)/kT}\Delta E_{g,Ge}(grade)/kT}{1 - e^{-\Delta E_{g,Ge}(grade)/kT}}\right\} \quad (6)$$

where the symbol "$\sim$" denotes a position-averaged quantity, N_{ab}^- is the ionized doping level in the base, and $\tilde{\eta} = \left(\widetilde{D_{nb}}\right)_{SiGe}/(D_{nb})_{Si} > 1$ is the minority electron diffusivity ratio between SiGe and Si.

It is clear from Equation 6 that $J_{C,SiGe}$ is exponentially dependent on the Ge content at the BE junction, Ge(x=0), and linearly dependent on the grading of Ge across the base. Therefore, a Ge profile shape change will exponentially vary $J_{C,SiGe}$. Also, it is noticeable that the thermal constant, kT is the denominator in the exponent terms, so all these bandgap effects will be exponentially varied with temperature, i.e. this function is thermally activated. The influence of the Ge-induced energy band offset on collector current density is contained entirely in the second term of this relation, and thus can be described as the SiGe current gain enhancement factor.

$$\frac{\beta_{SiGe}}{\beta_{Si}} \cong \frac{J_{C,SiGe}}{J_{C,Si}} = \frac{\widetilde{\gamma}\widetilde{\eta}\Delta E_{g,Ge}(grade)/kT e^{\Delta E_{g,Ge}(0)/kT}}{1 - e^{-\Delta E_{g,Ge}(grade)/kT}} \quad (7)$$

Ge-induced energy band offset at the EB junction ($\Delta E_{g,Ge}(0)$) also exerts a exponential influence on the gain increase of the device. In the case of "strong Ge grading" ($\Delta E_{g,Ge}(grade) >> kT$), characteristic of a triangular Ge profile, the exponential term on the denominator becomes very small and this factor approximately reduces to $\approx (\widetilde{\gamma}\widetilde{\eta}\Delta E_{g,Ge}(grade)/kT)e^{\Delta E_{g,Ge}(0)/kT}$. In the case of "weak Ge grading" ($\Delta E_{g,Ge}(grade) << kT$), characteristic of a box Ge profile, the SiGe current gain enhancement factor is shown

to be approximately $\widetilde{\gamma}\widetilde{\eta}e^{\Delta E_{g,Ge}(0)/kT}$. The output conductance, r_o, is an important design pa-

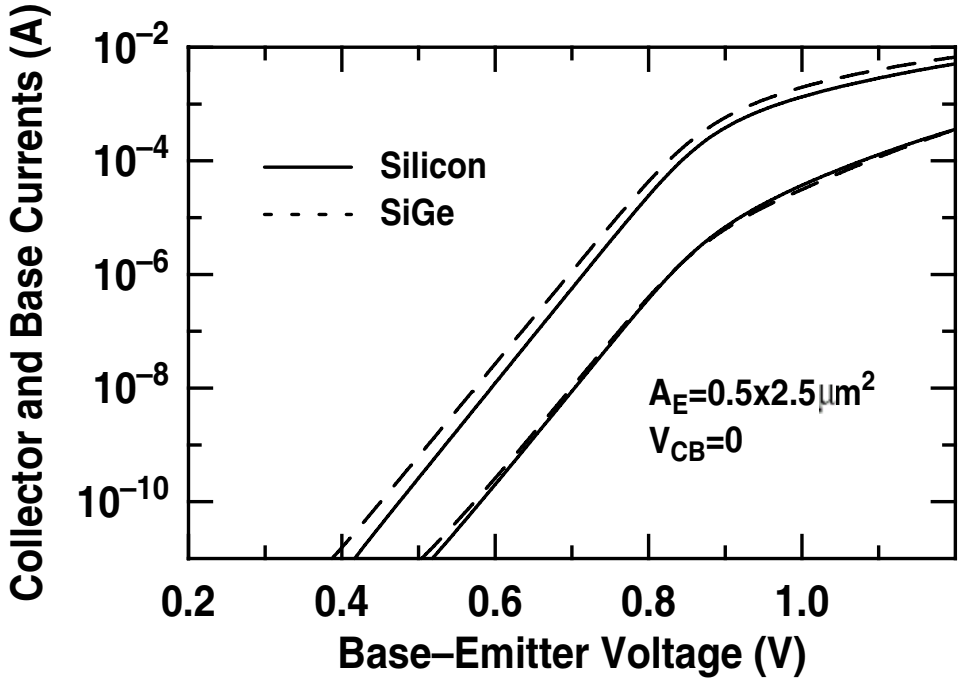

Figure 7: Representative Gummel plot for a SiGe HBT as compared to a Si BJT.

rameter for analog circuits and although ideally, it should be zero, it is well known that with increase in Collector-Base voltage (V_{CB}), the CB Space Charge Region (SCR) increases. This is because the CB junction is increasingly reverse-biased. The decrease in effective base width increases minority carrier concentration gradient across the base, which consequently increases $J_{C,SiGe}$, i.e. r_o decreases from the ideal infinity. This effect is called "Early Effect", and is measured by the "Early Voltage" (V_A), which is defined as,

$$V_A = J_C(0)\left\{\left.\frac{\partial J_C}{\partial V_{CB}}\right|_{V_{BE}}\right\}^{-1} - V_{BE} \approx \left\{\left.\frac{\partial J_C}{\partial W_b}\right|_{V_{BE}}\frac{\partial W_b}{\partial V_{CB}}\right\}^{-1} \tag{8}$$

And, consequently, the Early Voltage ratio between SiGe and Si, can be written as,

$$\left.\frac{V_{A,SiGe}}{V_{A,Si}}\right|_{V_{BE}} = e^{\Delta E_{g,Ge}(grade)/kT}\left[\frac{1-e^{-\Delta E_{g,Ge}(grade)/kT}}{\Delta E_{g,Ge}(grade)/kT}\right] \tag{9}$$

This relation shows that Ge-induced bandgap grading has an exponential influence of on Early voltage. Therefore two different components of the Ge profile in a SiGe HBT

provides separate ways for optimizing β and V_A, using $\Delta E_{g,Ge}(0)$ and $\Delta E_{g,Ge}(Grade)$, respectively. This property is lacking in standard Si BJTs, as the enhancement of one of these two factors fundamentally requires degradation of the other as they are both related to the base doping. Therefore, as the base doping is effectively decoupled from both β and V_A, the parameters can be maximized independent of each other, and this tradeoff in analog circuits is avoided and the important figure of merit $\beta \cdot V_A$ maximized.

The dynamic performance for SiGe HBTs are better than Si BJTs as well, which allows it to target high frequency niche applications in the RF and microwave circuit applications arena. The base transit time, τ_b, is a major delay that comprises a significant portion of the total delay time for bipolar transistors. However, this is improved in SiGe HBTs as there is a drift component added to the diffusion component in the carrier transport mechanism in the base, due to the Ge grading induced conduction band grading. τ_b for SiGe is given by

$$\frac{\tau_{b,SiGe}}{\tau_{b,Si}} = \frac{2}{\widetilde{\eta}} \frac{kT}{\Delta E_{g,Ge}(grade)} \left\{ 1 - \frac{kT}{\Delta E_{g,Ge}(grade)} \left[1 - e^{-\Delta E_{g,Ge}(grade)/kT} \right] \right\} \tag{10}$$

Additionally, since the emitter charge storage delay time (τ_e) is proportional to $1/\beta$, the higher β of a SiGe HBT will reduce this factor and further reduce delay.

$$\frac{\tau_{e,SiGe}}{\tau_{e,Si}} \simeq \frac{J_{C,Si}}{J_{C,SiGe}} = \frac{1 - e^{-\Delta E_{g,Ge}(grade)/kT}}{\widetilde{\gamma}\widetilde{\eta} \frac{\Delta E_{g,Ge}(grade)}{kT} e^{\Delta E_{g,Ge}(0)/kT}} \tag{11}$$

A standard figure-of-merit for dynamic transistor performance is the unity-gain cutoff frequency (f_T). For low-injection, this parameter can be written as

$$f_T = \frac{1}{2\pi} \left[\frac{1}{g_m}(C_{eb} + C_{cb}) + \tau_b + \tau_e + \frac{W_{CB}}{2v_{sat}} + r_c C_{cb} \right]^{-1} \tag{12}$$

As stated above and shown explicitly here in Equation (12), reduction of τ_b and τ_e will result in reduced overall transit time (τ_{ec}) and thus increase f_T. Likewise, the unity power-gain frequency (or, maximum oscillation frequency, f_{max}) will also improve since it is a function of f_T, given by

From Equation 12, it is clear that the reductions of both τ_b and τ_e will increase the f_T of the SiGe HBT over the Si BJT.

The maximum oscillation frequency, or f_{max}, another dynamic figure of merit, is also improved:

$$f_{max} = \sqrt{\frac{f_T}{8\pi C_{cb} r_b}} \tag{13}$$

where r_b is the *ac* base resistance and C_{cb} is the collector-base capacitance. The increase in f_T as well as a reduction in r_b aid in improving the f_{max} of the SiGe HBT.

The Ge grading in the base region of the SiGe significantly improves both f_T and f_{max}, and thus overall *ac* performance.

It is worth noting that that for Si BJTs, if doping in the base was increased, it would improve f_T a lot, as τ_b would decrease, but so would β, so there was another tradeoff. For SiGe, since β is improved by the Ge content in the base, although increase in base doping will decrease β, it would be offset to a much higher value than its Si BJT counterpart, allowing more room for device designers to optimize the transistor.

It is evident after this discussion that box profiles are good for enhancing β, but triangular profiles are better for V_A, f_T, and f_{max}. So, a compromise has to be reached between these profiles, and that is a trapezoidal.

1.4 Second Order Effects

Second Order Effects in SiGe HBTs will always exist and need to be understood well for optimal use of the device in circuit applications. Two effects will be summarized in this thesis. If not otherwise stated, the discussions will assume that the bipolar device in concern is NPN.

1.4.1 Ge-grading Effect

As was discussed earlier, the current gain of SiGe HBTs are exponentially dependent on the Ge(x=0). During medium injection regime, as J_C increases, there is a corresponding rise in V_{BE}, i.e. the forward bias across the EB junction increases and the EB Space Charge Region (SCR) shrinks. The thinner depletion region leads to the Ge content at the emitter

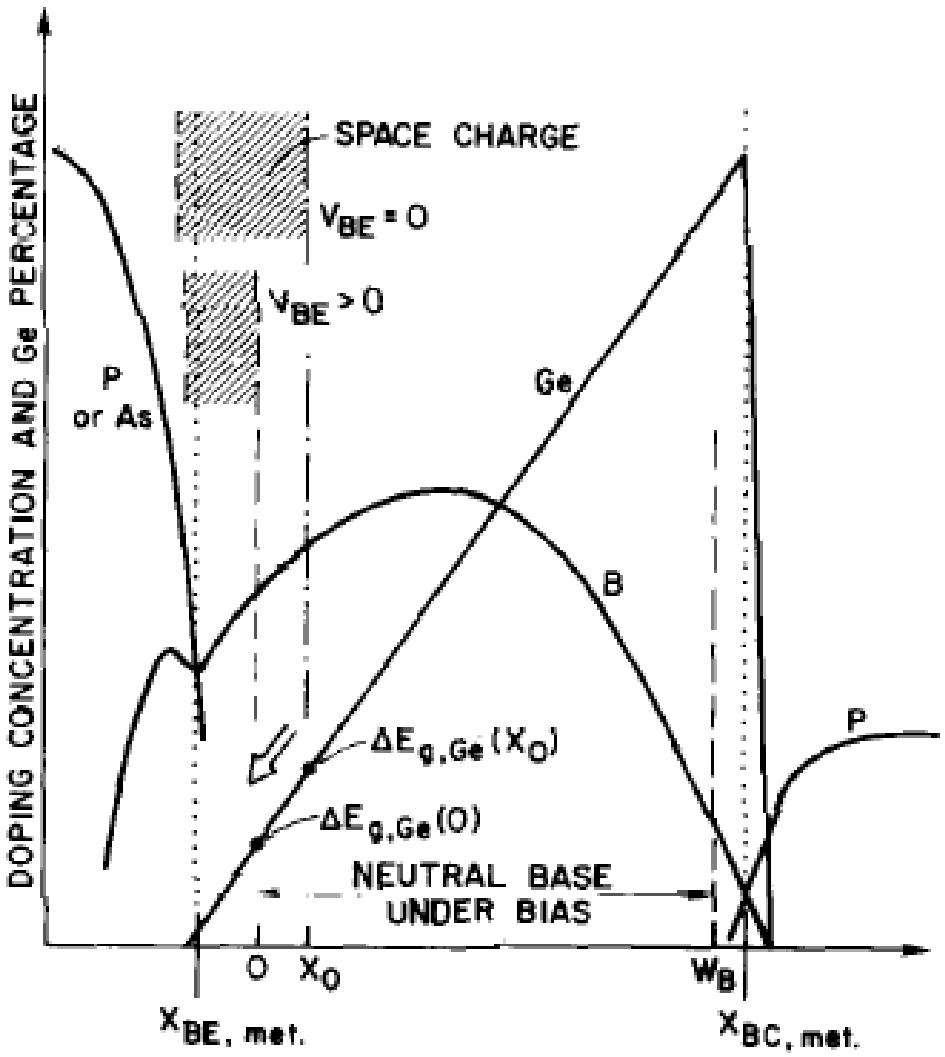

Figure 8: The Late Effect, [32].

end of the base to change and exponentially affect β. The Figure 8 illustrates this effect, called the inverse Early or "late" effect [32].

Now, for devices with highly graded Ge profiles, the change in Ge(x=0) with the late effect would be more, so the Ge grading effect is worse for highly graded profiles.

1.4.2 Tunneling Effect

It is worth mentioning at this point, when we are addressing non-high injection effects, that there is another effect that dominates at low injections, the tunneling effect. This is a purely

quantum mechanical effect that allows carriers to go through potential energy barriers from a filled energy state in the valence band to an empty one in the conduction band on th other side of the barrier which is at an equal energy level. This can be seen clearly in the Figure 9. For tunneling to occur, the width of the potential barrier, d, must be very thin, and it is significant for d<100 Angstroms, i.e. when the depletion width between the junctions in the transistor is $<10^{-6}$cm [10]. This effect can therefore, be easily reduced by increasing d, by placing an intrinsic Si layer between the junctions, the i-p-i base [3]. Tunneling is a breakdown mechanism in Zener diodes, and under reverse bias, as built-in voltage rises linearly with increase in reverse-bias voltage, depletion width changes less than linearly, thereby, allowing d to decrease and tunneling to take place. Tunneling currents are weakly dependent temperature, decreasing temperature decreases. Therefore, it has an opposite relationship with temperature compared to avalanching, another breakdown method, to be discussed below.

1.4.3 Heterojunction Barrier Effect

All HBTs experience heterojunction barrier effects (HBE). Simply, HBE arises from the inability of two physically adjacent semiconductors with different bandgaps to line up both their conduction and the valence bands, in other words, band misalignment. This band misalignment leads to formation of abrupt barriers at the EB and CB junctions of HBTs. The way the bands align, and the location of the abrupt barriers (in the conduction band, valence band, or both) is unique to different materials and does not change with temperature. For SiGe HBTs, with the wider bandgap Si emitter and collector and the narrower bandgap SiGe base, the barrier is present in the valence band. By varying the composition of the Ge in the base, the barrier can effectively be softened and the energy band modified [10].

The barrier is usually hidden by the SCR at the heterojunctions and do not create any problems, until exposed. At the CB junction, the barrier can have adverse effects, mainly

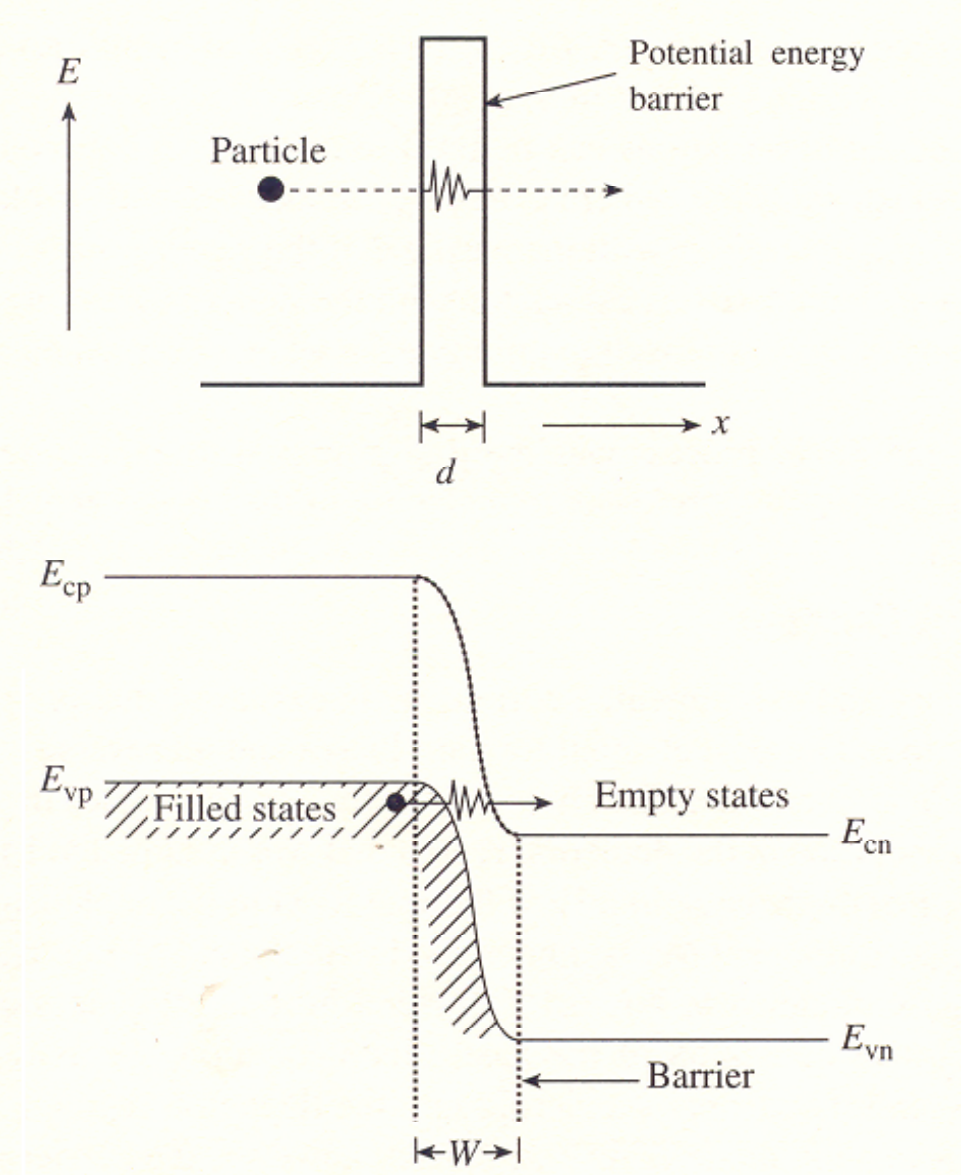

Figure 9: 2-D schematic of the tunneling process, [10].

at high injections. At all injections however, there can be HBE at the CB junction, if there exists a Ge-misplacement. This may happen if the Ge content approaches zero within the p-type. In a SiGe npn HBT, this may happen due to processing or fabrication issues such as excessive out-diffusion of the p-type base dopant (such as boron), during excessive thermal cycles beyond the Ge profile edge. Physically, this means that two p+ type semiconductors with different bandgaps are juxtaposed that may lead to an energy hump to occur in the conduction band at the germanium profile edge near the CB junction, called the parasitic conduction band [3]. The barrier can induce minority carrier pile-up in the base and severely degrade *dc* and *ac* performance of the transistor even at low J_C. However, this low J_C HBE is easily avoided by proper SiGe film growth, addition of an intrinsic Si layer between the base and the collector, called the emitter-cap layer [33], and other methods discussed in more detail in [3].

High injection HBE, is of more interest as it cannot be designed around easily and has adverse effects on the *dc* and *ac* performance of the HBT. High injection for Si-bipolar transistors is generally said to occur "when the local minority carrier density in the emitter, base, or collector region, approaches and then exceeds the local ionized doping level" [3]. The high injection effects are more serious in the collector region as the doping density there is lower than in the base or the emitter. The main effect of high injection is that J_C and J_B start to react non-ideally, that is they are not proportional to $e^{qV_{BE}/kT}$ any more. This non-ideality can be explained by quasi-saturation of base and emitter terminals, the Kirk effect, Webster-Rittner effect and quasi-saturation due to collector resistances. Among these, Kirk effect is the most significant. Physically, at high enough injections, the minority carrier concentration in the CB depletion region exceeds the space charge on the collector side of the region, and hence causes the whole region to collapse and the base to 'push out' into the collector. Now, we know that, J_C is proportional to $1/W_b$ and τ_b is proportional to $(1/{W_b}^2)$. Therefore, this increase in the base bandwidth (W_b) causes corresponding decrease in J_C, decrease in J_B, increase in τ_b and therefore, decrease in β and f_T.

The J_C at which there is onset of Kirk effect can be written as

$$J_{C(Kirk)} = qv_{sat}N_{DC}\left\{1 + \frac{2\epsilon(V_{CB} + \phi_{bi})}{qN_{DC}{W_C}^2}\right\} \tag{14}$$

where, v_{sat} is the saturation velocity of the carriers. In SiGe HBT, the collapse of the CB SCR unearths the HBE that was hidden at lower injections. This exposed offset in the valence band restricts hole injection into the collector. Hole accumulation at the CB junction end of the neutral base is accompanied by electron accumulation in the conduction band to maintain charge neutrality. This accumulation increases carrier recombination and in effect increases base current, exacerbating the performance degradation.

The onset of Kirk effect and hence the HBE can be pushed to higher J_C by increasing the collector doping, and also by retrograding Ge well into the collector, to soften the barrier (as discussed earlier) and reduce the HBE. However, these measures come with the penalties, as an increase in collector doping is accompanied by decreased breakdown voltage (BV_{CEO}) as there is an increase in electric field across CB junction and CB capacitance. This degrades the delay properties and peak f_T and f_{max}. This classic tradeoff between peak f_T and BV_{CEO} is reflected in the Johnson's limit, $f_T \cdot BV_{CEO}$ [27]. Also, increasing Ge content in the collector may introduce thermal stability concerns of the SiGe pseudomorphically grown film. Further details of retrograding and aggressive scaling of the base, and its effect on high injection effects can be seen in [34].

1.5 Breakdown Fundamentals

At high injections, if the collector doping is increased (to move $J_{C(Kirk)}$ to higher the J_C) the magnitude of the drift field within the CB-SCR, will cause conduction electrons in this region to obtain high kinetic energy. In the event that an electron of sufficient velocity collides with the lattice, excess energy may be transferred to an electron in the valence band, promoting this carrier to the conduction band and creating an electron-hole pair (EHP). This generation process is the inverse of the Auger effect, and is known as impact ionization [10]. Snowball effect follows the impact ionization, when one electron gives rise to

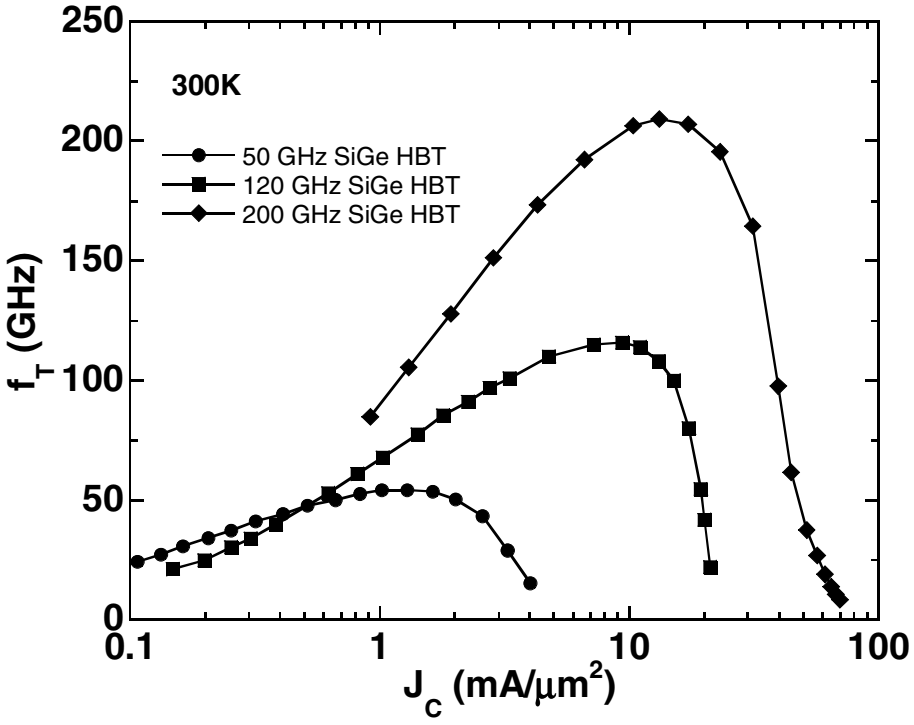

Figure 10: Cutoff frequency as a function of collector current density for three generations of SiGe HBT BiCMOS technology.

another, and the additional EHP creates more impact ionization, and effectively there is a "snowball" effect. As the reverse bias potential across the junction (VCB in a bipolar transistor) increases, the probability that each carrier in the depletion region will undergo an impact ionization event increases, eventually leading to junction breakdown. This probability is typically represented as the avalanche multiplication factor (M), which is the ratio of reverse-biased junction current without impact ionization to the junction current with impact ionization, or

$$M = I_{n,out}/I_{n,in} \tag{15}$$

Generally, M-1, instead of M is used to better describes the yield or efficiency of the collector current increase. This can be measured using forced-V_{BE} or the forced-I_E. Low injection data is better to use and it is safer to use the forced-I_E method because then the total amount of current injected in the CB SCR will always be limited by I_E [3]. The

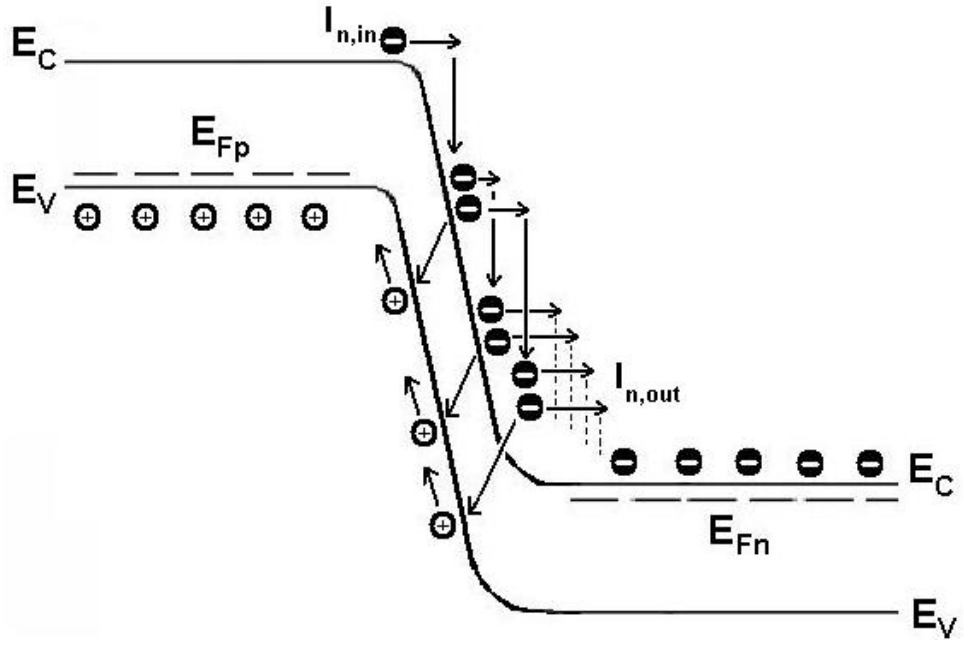

Figure 11: Schematic illustration of the avalanche multiplication process in a reversed bias p-n junction.

forced-I_E method can be seen in Figure 12, where,

$$M - 1 = \frac{I_C(V_{CB})}{I_E - I_B(V_{BE}@V_{CB} = 0)} - 1 \tag{16}$$

Increasing the collector doping, in order to achieve higher device performance, increases the rate of avalanche multiplication within the device and thus reduces its breakdown voltage. Table 1 shows that open-emitter reverse bias collector junction breakdown voltage (BV_{CBO}) decreases from 10.5 V to 5.5 V from IBM 5-8HP as peak f_T increases from 50 GHz to 200 GHz. This tradeoff between peak f_T and breakdown voltage in SiGe HBT device design. is a fundamental limit described better by the (larger) $BV_{CES} \cdot f_T$ product ($BV_{CES} \approx BV_{CBO}$) than the traditional $BV_{CEO} \cdot f_T$ product [41]. At lower temperatures, since the lattice scattering reduces, higher velocities can be reached by carriers, thereby increasing the rate of avalanche, increasing M-1 and decreasing breakdown voltages.

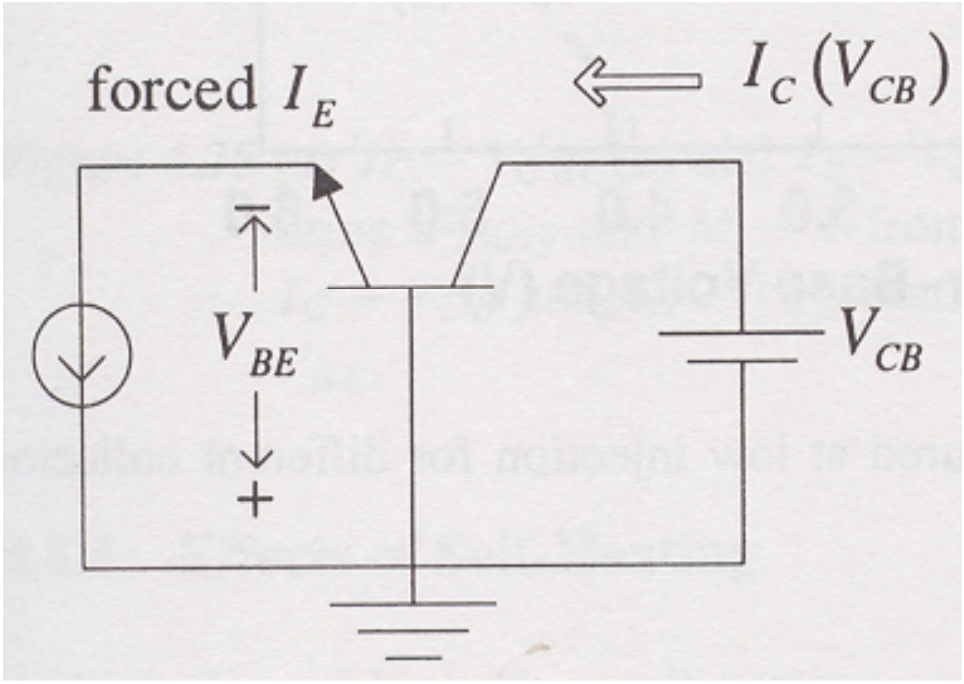

Figure 12: Forced I_E method for M-1 calculation, [10].

1.6 Summary

This chapter sets the ground for the thesis. The motivation for using SiGe HBT BiCMOS technology over its contenders, such as the III-V device technologies for high frequency wireless applications were presented. The need for further studies in cryogenic characterization of the various existing technologies was mentioned. A brief overview of the existing technologies and the device physics behind SiGe HBTs was given, and the various device design tradeoffs that exist for the optimization of SiGe HBTs were discussed. Second order phenomenon and breakdown voltage issues were also discussed.

CHAPTER II

CRYOGENIC OPERATION OF SIGE HBTS

2.1 Introduction

SiGe HBTs have various advantages over traditional silicon-bipolar transistors when it comes to cryogenic operation. Silicon bipolar transistors static characteristics in terms of β, and V_A degrade with decrease in temperature, whereas those for SiGe HBTs improve. However, second order effects, such as HBE, Ge-grading, and tunneling, may decrease the *dc* operating regime of a SiGe HBT drastically with cooling. Most SiGe HBTs are not optimized for low temperature operation and for cryogenic circuit applications that may use these unoptimized devices, it is important to know the trends and variations of these and more parameters at low temperatures.

This chapter, will first discuss, theoretically, which parameters might be affected over temperature and how. Experimental data will then be presented to verify the concepts. The technology that will be presented will be IBM's first generation SiGe HBT BiCMOS, called IBM 5AM. This is a replica of the IBM 5HP technology with 50GHz peak f_T. Results for both flavors of this technology, High Performance and High Breakdown will be presented and compared.

2.2 Background

Cryogenic operation of SiGe HBTs is in many ways similar to that of their Si counterparts. This is because many of the device parameters and figure of merits for both types of bipolar transistors are band edge triggered, i.e. they depend exponentially on changes in band energy levels divided by the thermal constant, kT. Therefore, in effect, they depend

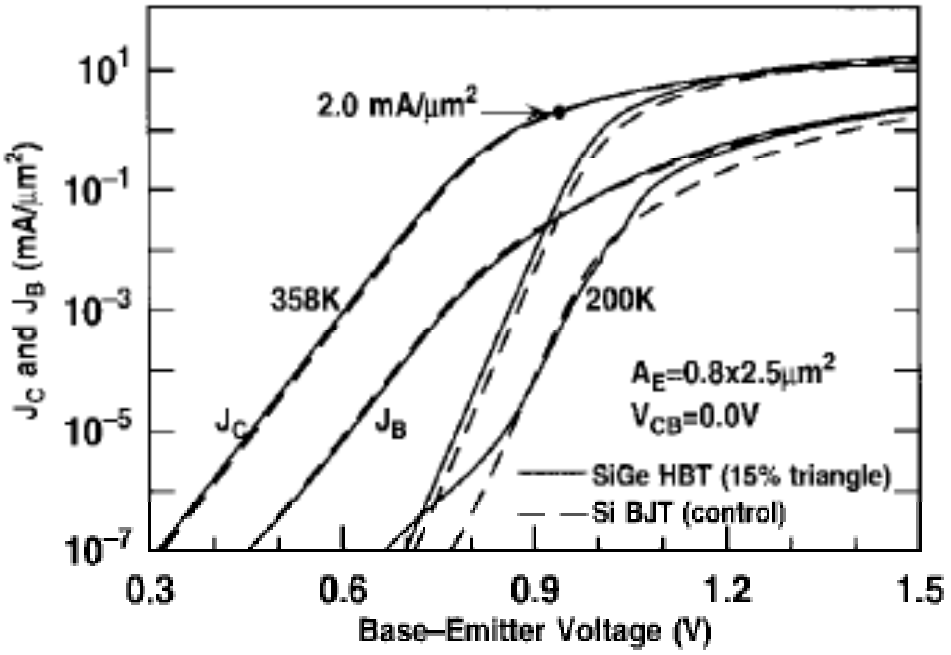

Figure 13: Gummel characteristic for a first generation SiGe at different temperatures.

exponentially on temperature changes measured in Kelvin. A function that has this characteristic is generally called 'thermally activated'. Therefore, depending on the position of the kT in the equations describing these functions, the dc performance of these devices may improve or degrade with temperature, and differ from each other.

The Figure 13 shows how the gummel characteristic of a first generation SiGe HBT varies with temperature. As temperature drops, it is clearly observed from the gummel characteristic, that for fixed bias currents, base-emitter voltage, V_{BE}, increases. This is because the built-in voltage rises with cooling. The built-in voltage is dependent on temperature through its dependence on the thermally activated intrinsic carrier density.

This trend implies that J_C should be lower for lower temperatures at fixed V_{BE}. The collector current density can be written as

$$J_{C,SiGe} \cong \frac{qD_{nb}}{p_B x_T}\left(e^{qV_{BE}/kT}-1\right) n_{io}^2 \left\{ \frac{\widetilde{\gamma}\widetilde{\eta} e^{\Delta E_{gb}^{app}/kT} e^{\Delta E_{g,Ge}(0)/kT} \Delta E_{g,Ge}(grade)/kT}{1-e^{-\Delta E_{g,Ge}(grade)/kT} + \frac{1}{kT}\left(\frac{W_B}{x_T}-1\right) e^{-\Delta E_{g,Ge}(grade)/kT}} \right\} \tag{17}$$

Transconductance, g_m, which is also the slope of the gummel characteristic, increases with decrease in temperature. We get g_m as a function of temperature by deriving Equation 17 with respect to V_{BE},

$$g_m = \frac{\delta I_C}{\delta V_{BE}} \cong \frac{qI_C}{kT}\alpha\frac{q}{kT}e^q V_{BE}/kT \tag{18}$$

Though current density at constant bias drops with cooling, current gain for SiGe HBTs increases quasi-exponentially at low temperatures. This is because current gain depends exponentially on the band offset, $\Delta E_{g,Ge}(0)$, that is created at the EB junction and is therefore, thermally activated. The offset is created as the effective bandgap narrowing of the base due to doping, couples with that caused by the presence of Ge in the base, and exceeds the bandgap narrowing of the emitter. The current gain as a function of temperature was introduced in Chapter 1 in Equation 7.

Cooling affects emitter, collector, and base resistances negatively. This is because as temperature goes down, carriers in the semiconductor tend to "freeze-out", i.e. the number of carriers available drops below the number expected from the level of doping in the semiconductor. Consequently, resistance increases. The emitter and extrinsic base regions are usually doped higher than the Mott transition (about $3\text{x}10^{18}\text{cm}^{-3}$ for boron in Si), the doping level above which, the probability of freeze-out becomes negligible, [3]. The carrier concentrations there remain unaffected in these regions as compared to the case in the lighter doped intrinsic base and collector regions. Base freeze-out is usually severe at temperatures below 200K and is characterized by the sharp increase in pinched base sheet resistance [3]. Collector freeze-out is also severe at low temperatures, and leads to quasi-saturation, which cause premature Current Gain roll-offs. However, the sub-collector region is heavily doped and so at high injections, when the depletion region is 'pushed out' to the sub-collector, due to Kirk effect, the collector resistance drops significantly.

For extrinsic collector and extrinsic base regions, the variations in carrier transport between the metal and the semiconductor through the ohmic contact may change the resistance as well. The carrier transport mechanism through the ohmic contact is via tunneling

mechanism [10].

Early voltage, V_A is also a function of temperature. It was written in Equation 9 in Chapter 1. It can be seen from the equation that V_A has an inverse relationship with temperature. With cooling, the CB SCR retains its ionization and requires higher minority carrier injections to decrease the neutral base width. Therefore, the early voltage decreases.

Temperature also affects the magnitude and onset of second order phenomena in SiGe HBTs. As discussed above, the Ge-grading effect affects J_C via the change of Ge content at the EB junction. Now as J_C is a thermally activated function, Equation 6, with cooling, the effects of Ge-grading will worsen. Ge-grading effect should therefore make the current gain roll-off at medium injections faster, with respect to V_{BE}, with decrease in temperature.

The magnitude of the HBE will also be more pronounced at lower temperatures, as the carrier transport currents are thermally activated functions of the barrier height [6], [34], [42], [43].

The onset of Kirk effect, hence, HBE should occur at higher J_C with decreasing temperature. This is because $J_{C(Kirk)}$ depends on saturation velocity, v_{sat}, as depicted in Equation 14, which increases moderately with cooling, increasing, $J_{C(Kirk)}$.

Tunneling current negligibly decreases with cooling, however, it becomes the dominant non-ideal base current at low temperatures at low injections. The effect here is linked to the fact that the emitter doping is very high in SiGe HBTs, which leads to high electric fields across the EB junction. Now, at low temperatures, even at relatively high V_{BE} drops across the EB junction, there is no carrier injection from the emitter into the base as the built in voltage is very high. Tunneling of electrons however can occur from filled states in the conduction band of the emitter tunnel into the unfilled states in the valence band of the base leading to base current leakage as holes have to enter from the external source to maintain charge neutrality. These carrier tunneling processes can be band-to-band or occur through more complex trap-assisted methods, but in any case leads to high base leakage currents that can kill the current gain at low injections at low temperatures.

At very low temperatures, close to Helium boiling point, of 4K, collector current leakage can also start occurring, and that is usually due to complex trap-assisted tunneling methods. Details are discussed in [6].

2.3 Static Characteristics of First Generation SiGe HBTs

2.3.1 Experimental Setup

In order to prove all the concepts developed so far and to try and gain deeper understanding of the device physics behind cryogenic operation of SiGe HBTs, a first generation IBM SiGe High Performance HBT with emitter area of 0.5x1.0μm^2 was characterized (dc) over a wide temperature range. Data was collected at five temperature points, including 300K, 231K, 162K, 93K, and 43K. At each temperature point, gummel characteristics, output characteristics (forced V_{BE}, forced I_B, and forced I_E methods [3]), and other specialized characteristics were collected for extraction of terminal resistances (emitter resistance, extrinsic collector resistance, and extrinsic base resistance). This study will mainly focus on the gummel and the output characteristics and the parameters that can be extracted from these measurements. The biasing schemes for the gummel and the output characteristics can be seen in Figure 14.

The system that was used for this experiment was a closed loop cryostat that uses an expander and a Helium compressor to achieve near liquid He temperatures. It is capable of operating within the range of 300K-10K. The on-wafer die with the wanted device was diced, wire-bonded to a 28-pin DIP package, and inserted into the 40-pin DIP socket of the cryostat. The cryostat's fan-out board was connected to the HP 4155 using cables. HP 4155 (Figure 15) was used to bias and measure the different characteristics of the device.

2.3.2 High Performance Results and Discussion

Figure 16 shows the variation of gummel characteristics over temperature from 300K to 43K for the 5AM HP device. It is clear that with cooling, V_{BE} at constant J_C bias, g_m (determined by the slope of the gummel) and β (Figure 17) monotonically increase, as

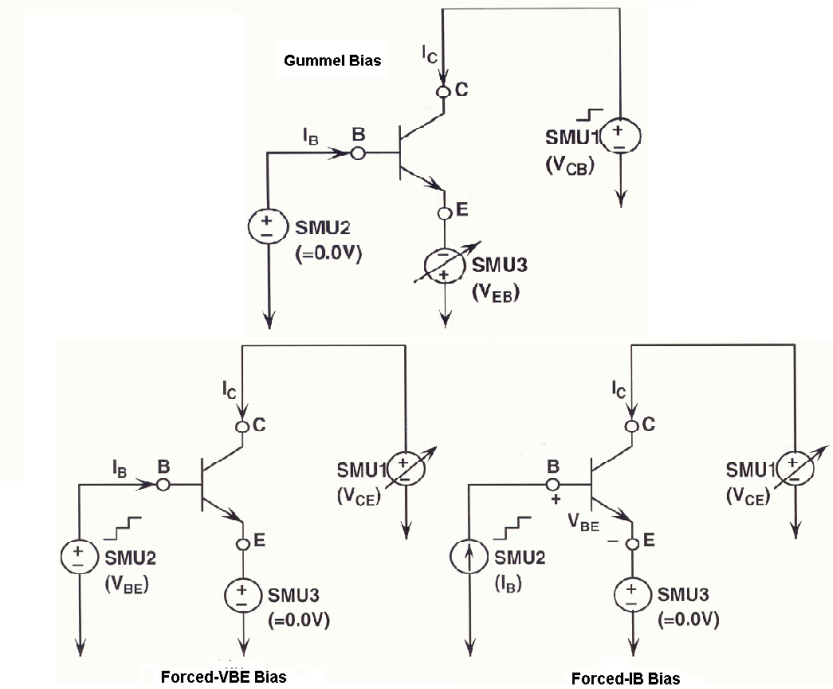

Figure 14: Biasing conditions for the Gummel and Output Characteristics.

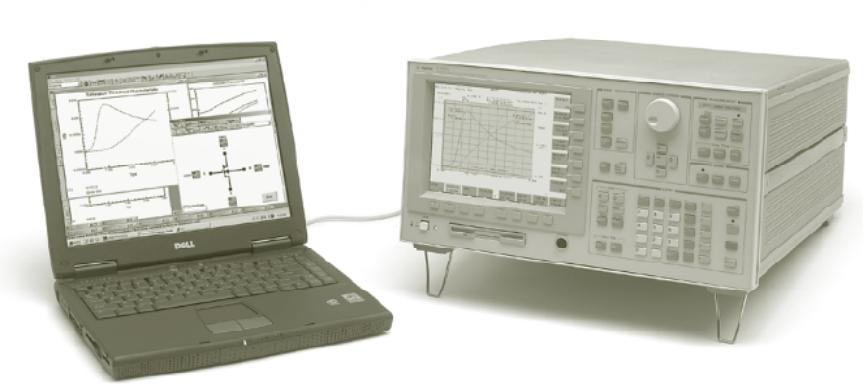

Figure 15: HP4155.

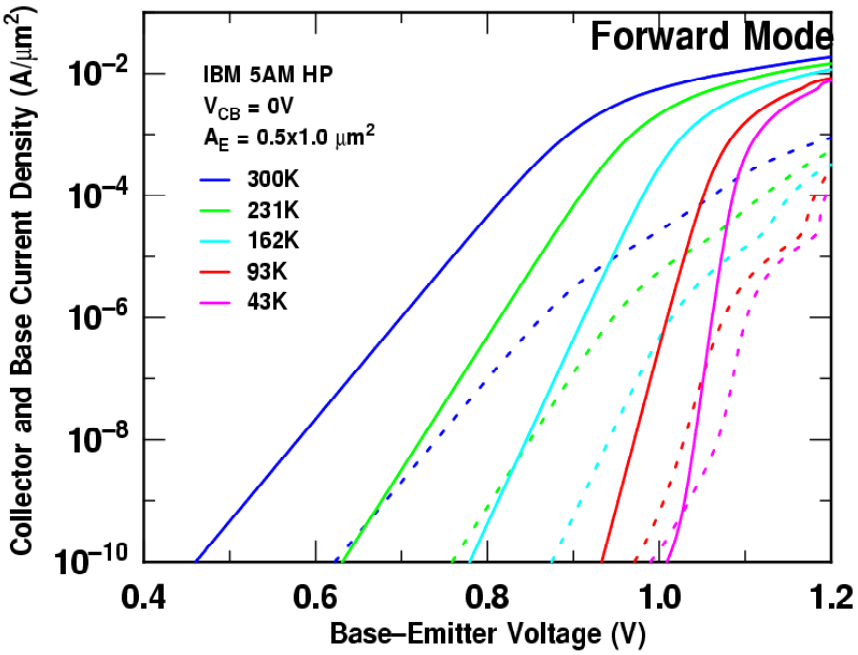

Figure 16: Gummel Characteristic of IBM 5AM HP at different temperatures.

suggested by theory. J_C can be seen to start rolling off softly at around 10^{-5}A/μm^2 and then sharply degrade at around 3mA/μm^2 in the 300K gummel in Figure 16. The trend remains similar for gummels at lower temperatures, with slight changes of current levels. These J_C degradation values can be seen to clearly coincide with the values at which β starts to softly roll-off and later sharply degrade in Figure 17, especially for lower temperature data. The roll-off of J_C and β can therefore be divided into two distinct stages, soft roll-off at medium injection regime, and sharp degradation at a high injection region. This differentiation was discussed in detail in [32], [34], [6], where the soft roll-off was attributed to Ge-grading effect, and the sharp degradation to Kirk effect and HBE. The medium injection drop gets steeper as temperature drops, indicating that the Ge-grading effect gets worse, as was predicted by theory.

To illustrate these roll-off effects better and investigate them further, it is important to look at the J_B behavior over temperature from the gummel characteristic plot as well. J_B seems to roll off at the same point as J_C but instead of flattening out at higher injections,

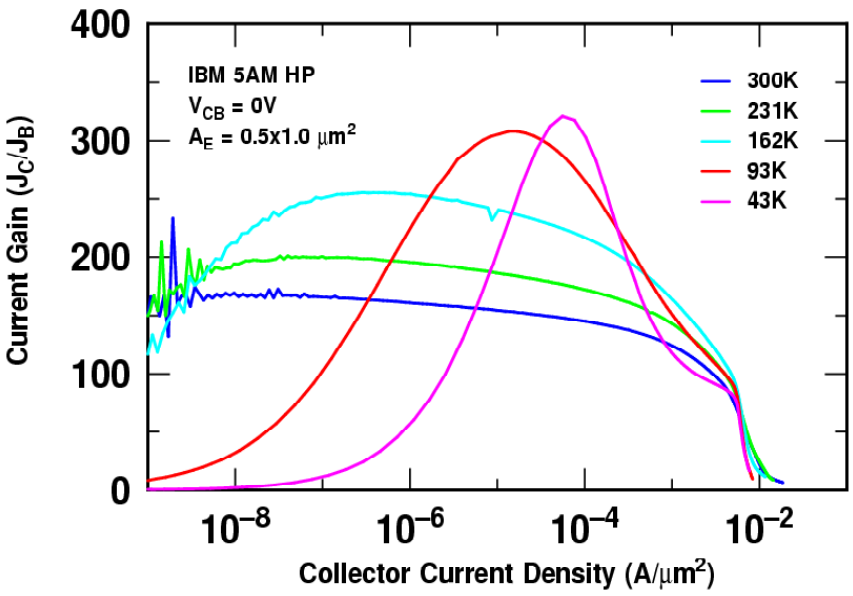

Figure 17: Current Gain for IBM 5AM HP at different temperatures.

it jumps, as predicted by the onset of Kirk and HBE effect. Also, the medium injection roll-off of J_B cannot be attributed to Ge-grading effect, as that affects J_C. Therefore, the J_B roll-off must be due to quasi-saturation of the base at high V_{BE} bias. Now, in order to verify this, it is best to have a look at Figure 18, which shows the slope of the gummel (for both J_B, $\frac{d(logJ_B)}{dV_{BE}}$, and J_C, $\frac{d(logJ_C)}{dV_{BE}}$) vs. J_C overlaid with the $\beta - J_C$ plot at 300K. It can be seen that at around 10^{-5}A/μm^2, when J_C starts to roll off in the gummel, $\frac{d(logJ_C)}{dV_{BE}}$ in Figure 18 starts to degrade faster than $\frac{d(logJ_B)}{dV_{BE}}$. This proves that Ge-grading effect coupled with quasi-saturation of the emitter and base regions cause J_C to roll-off faster than J_B, which is only affected by quasi-saturation. This effect gets clearer at lower temperatures. Now, as $J_{C(Kirk)}$ is reached, around 3mA/μm^{-2}, a sharp rise $\frac{d(logJ_B)}{dV_{BE}}$ is noticed as well as a sharp drop $\frac{d(logJ_C)}{dV_{BE}}$. This can be attributed to the "accumulation of holes in the base region due to the barrier onset" [34]. To prove that this is truly HBE, we have the slope of gummel vs J_C for V_{CB}=1V, which should increase the reverse bias on the CB junction, and therefore cause a shift in $J_{C(Kirk)}$ to higher J_C. This can be seen in Figure 21. The $J_{C(Kirk)}$, is clearly shifted to higher injection, therefore proving that HBE and Kirk effect coincide and occurs

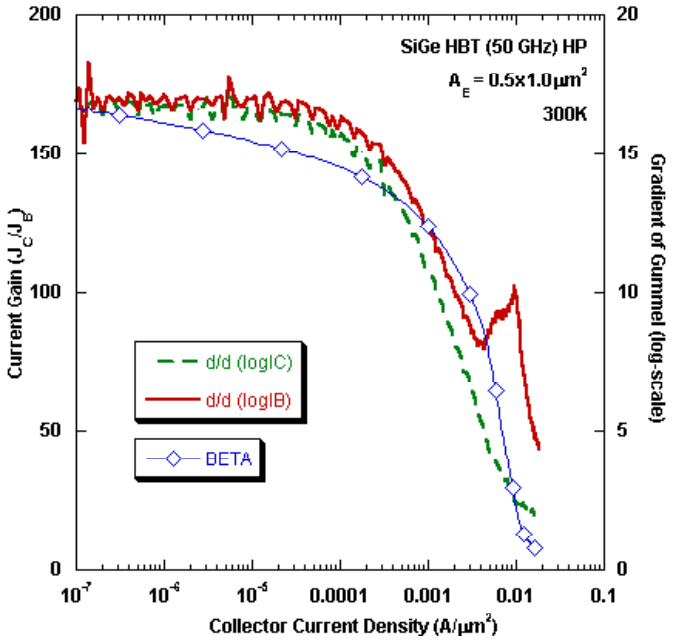

Figure 18: Slope of Gummel Characteristic vs. Collector Current Density for IBM 5AM HP at T=300K.

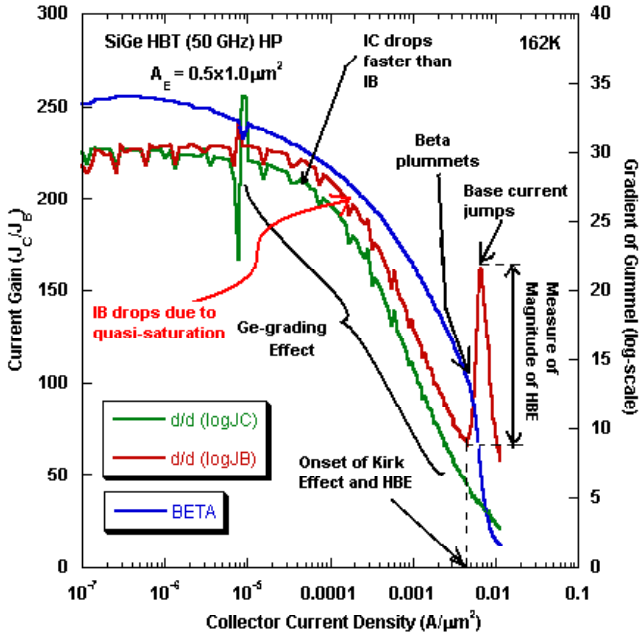

Figure 19: Slope of Gummel Characteristic vs. Collector Current Density for IBM 5AM HP at T=162K.

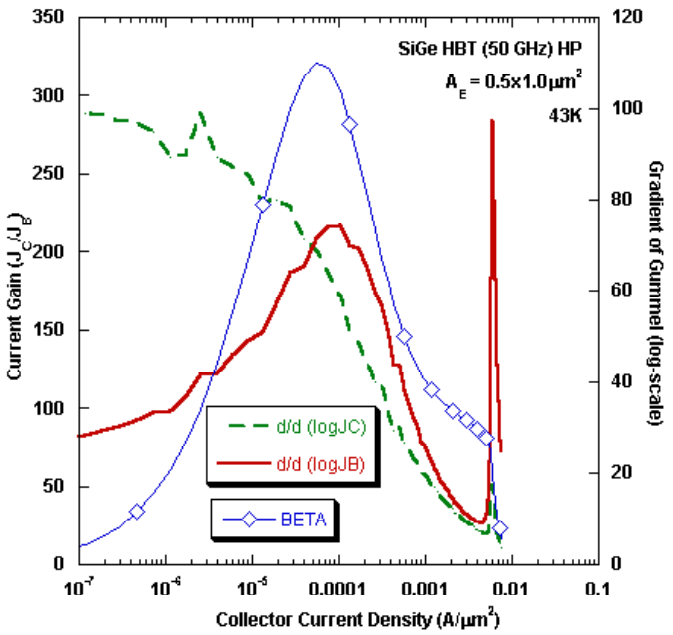

Figure 20: Slope of Gummel Characteristic vs. Collector Current Density for IBM 5AM HP at T=43K.

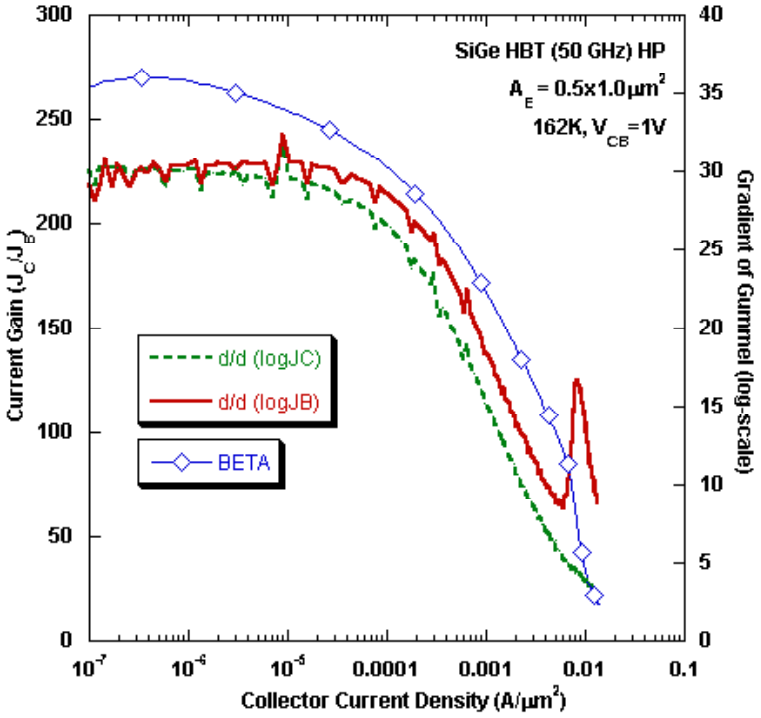

Figure 21: Slope of Gummel for IBM AM HP at 162K under a collector-emitter bias of 1V.

at around 3mA/μm^2.

The magnitude of HBE can therefore be a function of the change in magnitude of $\frac{d(logJ_B)}{dV_{BE}}$ at JC(Kirk). We can see that this increases from 5V$^-$1 to 10V$^-$1 to 95V$^-$1 as temperature drops from 300K to 162K to 43K (Figures 18, 19, and 20) i.e. HBE effect is worsened as temperature drops, just as predicted. Also, if a closer look is taken, the $J_{C(Kirk)}$), determined by the J_C at which $\frac{d(logJ_B)}{dV_{BE}}$ rises in Figure 18, increases, as can be seen when compared to Figures 19, and 20. It can be seen to shift over temperature, from 2mA/μm^2 to 3mA/μm^2 to 4mA/μm^2 as temperature goes down from 300K to 162K to 43K. Therefore, $J_{C(Kirk)}$ is also shown to increase with temperature drop, as was suggested by theory.

Most of these above roll-off concepts mentioned above are summarized pictorially in Figure **??**.

With decrease in temperature, we can also notice that the $\frac{d(logJ_B)}{dV_{BE}}$ from J_C roll-off to HBE onset gets larger (10/V to 20/V to 70/V as temperature changes from 300K to 162K to 43K). This indicates that the roll-off due to quasi-saturation of the base gets stronger with decrease in temperature. This effect is also clear from the gummel, where the J_B curve can be seen to flatten out more strongly before jumping up strongly, as Kirk effect takes place, at lower temperatures. This effect can be attributed to higher base resistances due to base freeze-out, which apparently increases with decrease in temperature, just as was predicted by theory.

The base current at lower temperatures, become increasingly non-ideal and leaky at low injections. This can be seen in both the gummel characteristic plots and the slope plots, and can be explained by the tunneling effect, which becomes the dominant base current mechanism as temperature decreases. This tunneling effect explains the shape of the $\beta - J_C$ plot, as it becomes increasingly bell-shaped with drop in temperature, and there is a very slight shift of the peak to the right. This would mean that the roll-off of gain and current density due to Ge-grading onsets stay constant over temperature.

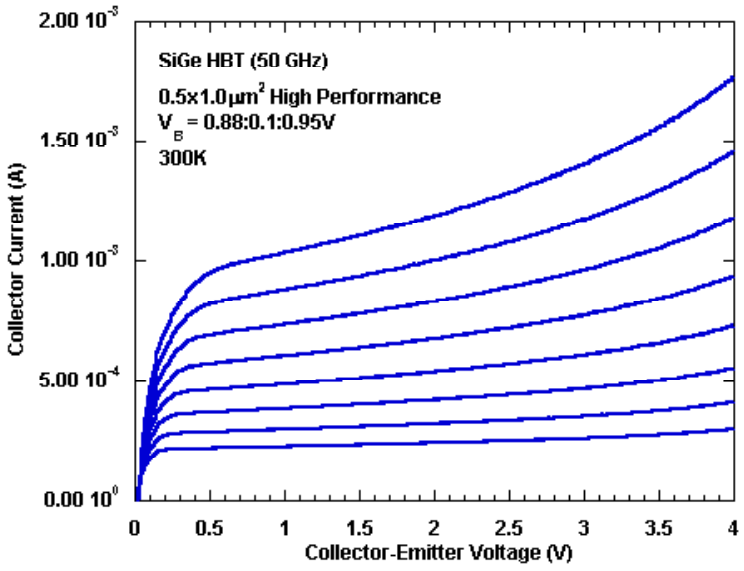

Figure 22: Forced V_{BE} Output Characteristic of IBM 5AM HP at T=300K.

Figures 22 and 23 show how the forced-V_{BE} output characteristics change over temperature.

The Early Voltage, V_A, can be found from these output characteristics using the technique depicted in Figure 24. This method works best for low injections as at high injections, second-order effects such as Ge-grading, HBE, self-heating, etc. come into play and the results are questionable [3].

The V_A is expected to increase and it does as temperature drops.

The M-1 value over temperature can be extracted from both forced V_{BE} and forced I_E output characteristic, with pros and cons for both as is described in detail in [**?**]. In this case, a forced V_{BE} output characteristic was used.

M-1 should increases as temperature drops, as the lattice scattering of avalanching electrons are reduced, meaning the electrons reach high velocities fast, and cause avalanche multiplication to increase, increasing M-1.

The breakdown voltage, BV_{CEO}, can be extracted from the forced I_B output characteristic plot taken at very low injections, and extrapolating the avalanching currents to the

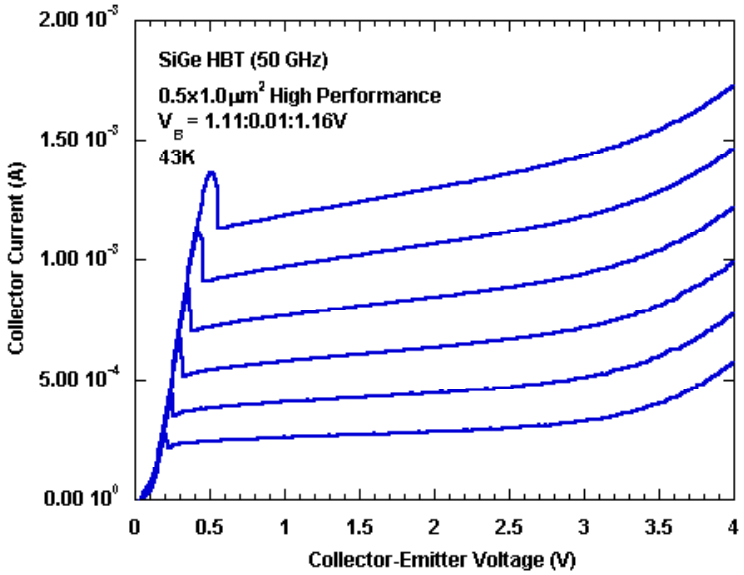

Figure 23: Forced V_{BE} Output Characteristic of IBM 5AM HP at T=43K.

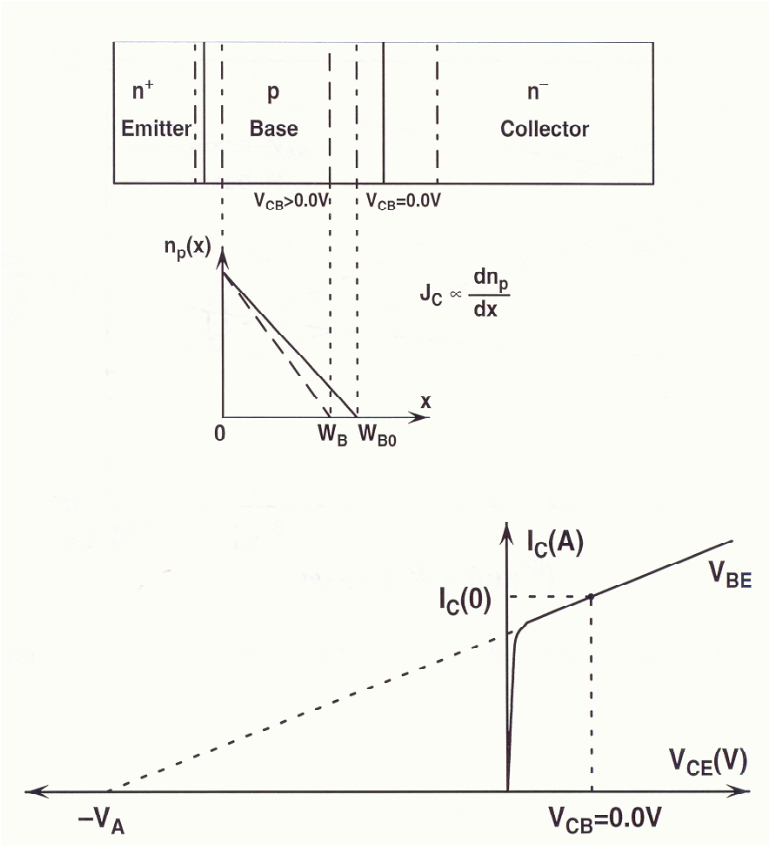

Figure 24: Early Voltage Extraction.

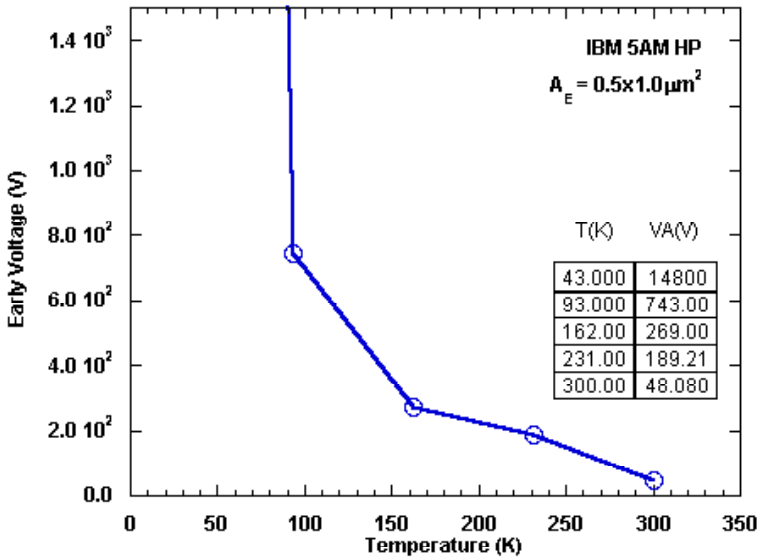

Figure 25: Variation of Early Voltage, V_A, with temperature for IBM 5AM HP.

x-intercept of the $I_C - V_{CE}$ plot. This x-intercept is the BV_{CEO}. It can also be extracted using the definition of BV_{CEO}, i.e. when $(M-1)\cdot\beta$=1, as discussed in detail in [3]. The extracted BV_{CEO} is seen to decrease as temperature drops, which is consistent with the M-1 results, and theory described above.

At high injection, the forced-I_B output characteristics show current gain degradation, as the input I_B are of the same order as the output I_C as can be, and 30 seen in Figures 28, 29, and 30. It is noticeable that V_{BE} drops as V_{CE} is increased. This is because of self-heating effects [3], which increases thermally activated recombination across the base and consequently causes I_B to increase, as holes enter through external source to maintain charge neutrality. But as the measurement is a forced-I_B measurement, the HP 4155, that controls the I_B through modulating V_{BE}, decreases it, in order to maintain the constant level of I_B. Since self heating is thermally induced, its effect decreases as temperature is reduced, which is obvious as the slope of V_{BE} with respect to V_{CE} approaches 0 in Figure 30 as opposed to what is seen in Figure 28 and 29.

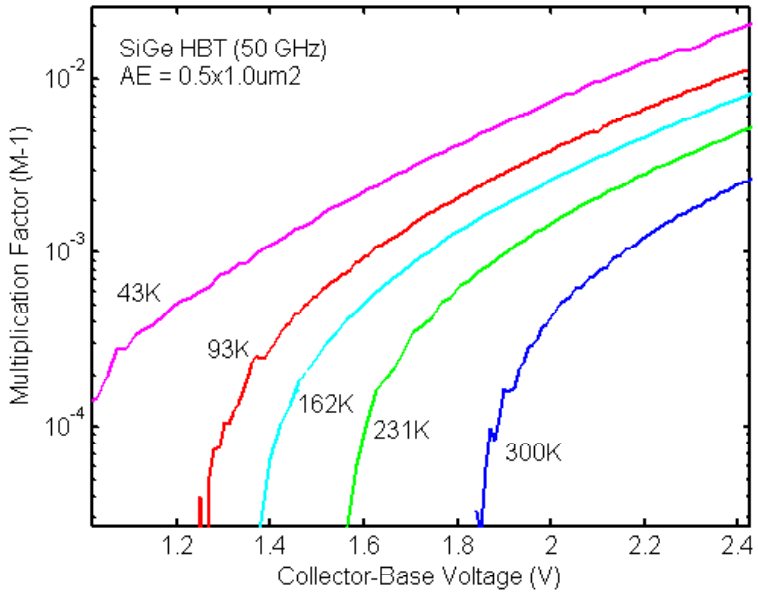

Figure 26: Variation of Avalanche Factor, M-1, with temperature for IBM 5AM HP.

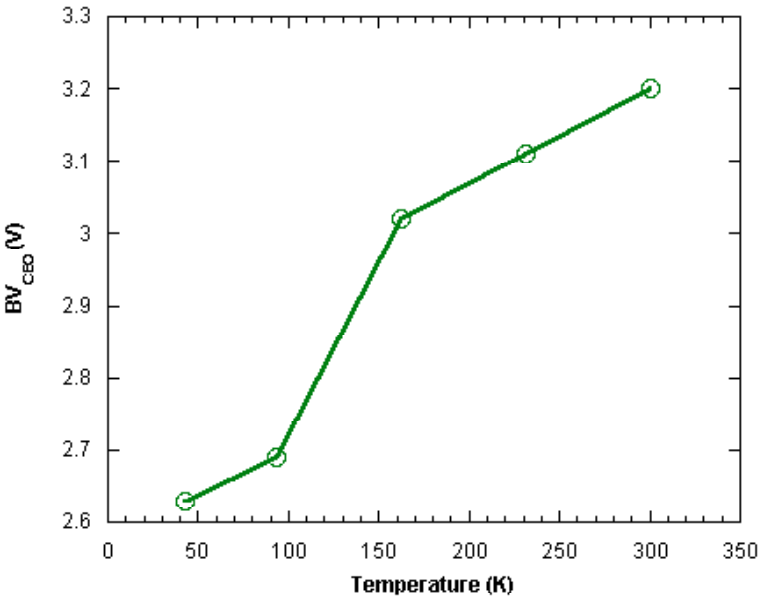

Figure 27: Variation of BV_{CEO} with temperature for IBM 5AM HP.

.

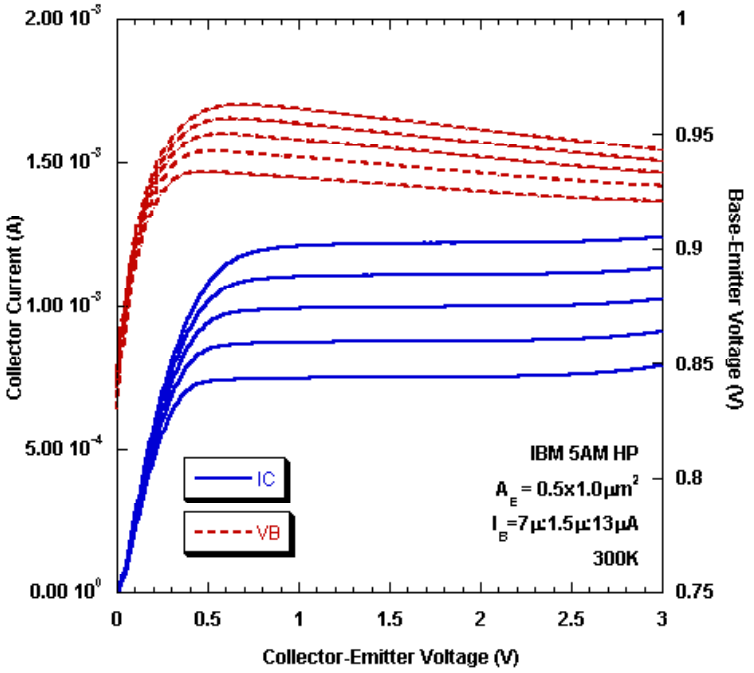

Figure 28: Forced I_B Output Characteristic of IBM 5AM HP at high injection at T=300K.

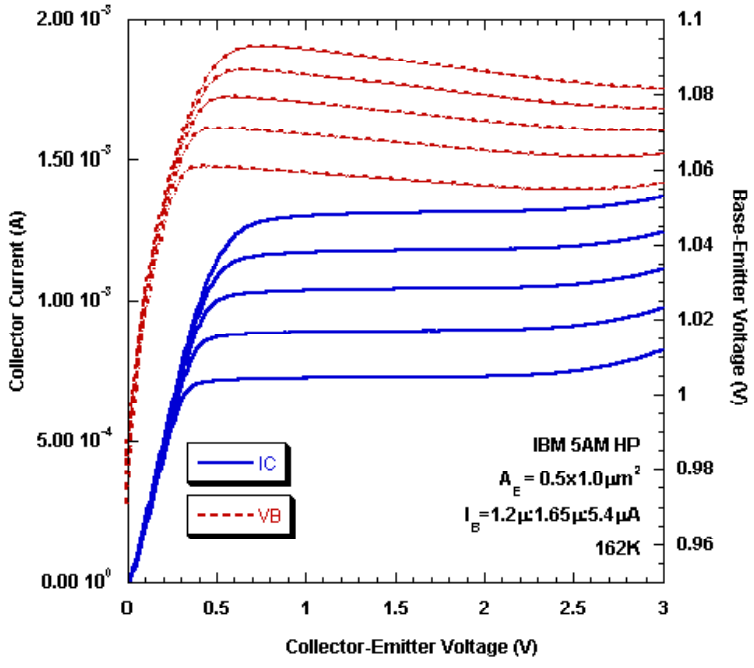

Figure 29: Forced I_B Output Characteristic of IBM 5AM HP at high injection at T=162K.

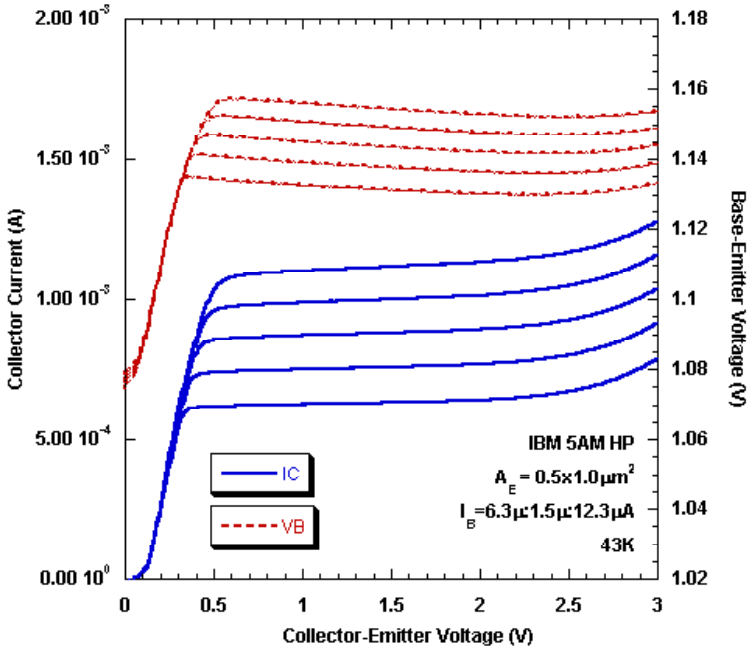

Figure 30: Forced I_B Output Characteristic of IBM 5AM HP at high injection at T=43K.

It is interesting to note that there lies a major shape difference between the high injection forced I_B and forced V_{BE} output characteristics. There is a clear formation non-ideal collector currents in the form of negative differential resistance regions (NDR) in the forced V_BE output characteristic plot at low temperatures (Figure 39. These occur at the edge of quasi-saturation and seem to disappear for higher temperatures (Figure 38), lower injections, and under forced-I_B mode (Figure 44). This negative slope of the collector current with respect to V_CE was also observed in [45], but it was reported to be seen in the forced I_B mode instead.

2.3.3 High Breakdown Results and Discussion

High Breakdown devices, as described earlier, are a different flavor of the same technology, which is optimized for higher breakdown voltages, achieved through an decrease in collector doping.

The gummel characteristic plots for the IBM 5AM High Breakdown (HB) device are presented in Figure 31 and the $\beta - J_C$ plots over temperature are presented in Figure 32.

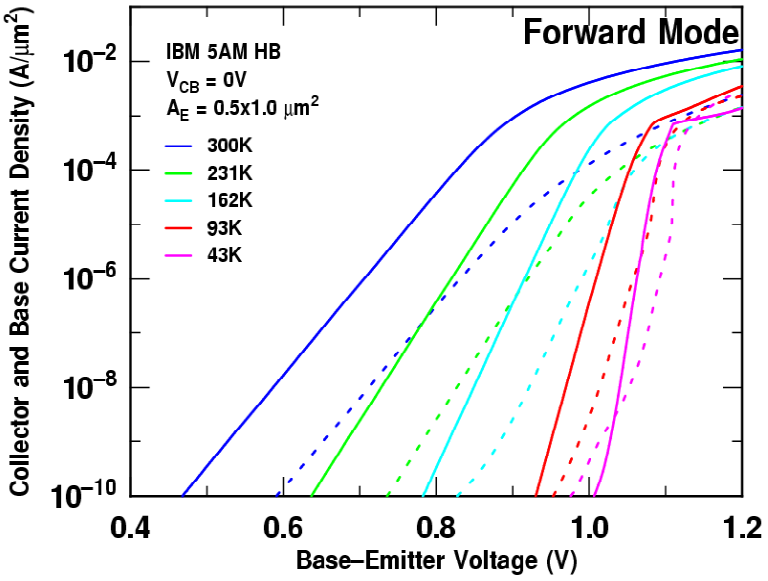

Figure 31: Gummel Characteristic of IBM 5AM HB at different temperatures.

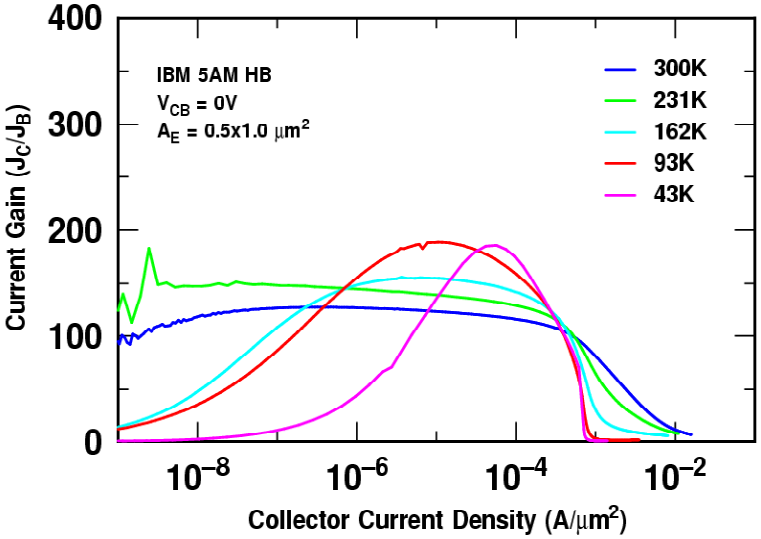

Figure 32: Current Gain for IBM 5AM HB at different temperatures.

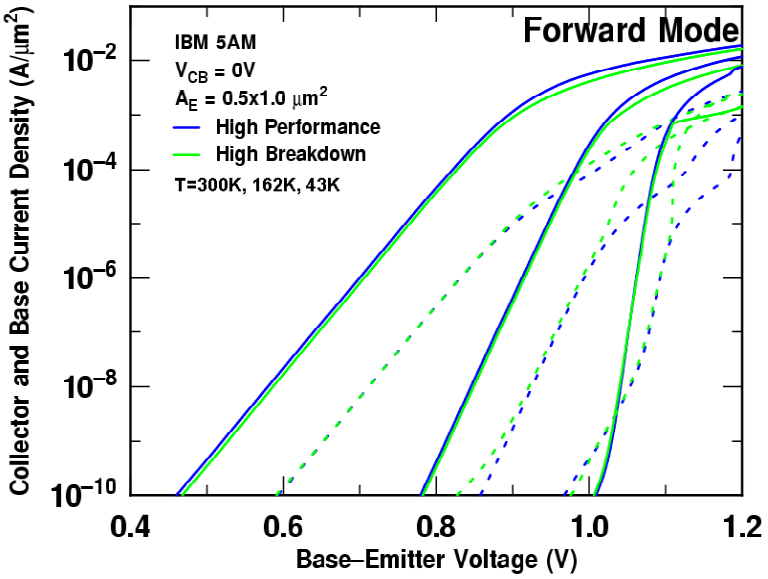

Figure 33: Comparison of Gummel Characteristics of IBM 5AM HP and HB at different temperatures.

It can be seen that most of the temperature trends including the current, gain, transconductance, built-in voltage, Ge-grading effect, and tunneling effect, trends follow closely with what was observed for IBM 5AM HP above, except for a few key differences, and these become clear when they are overlaid with the gummel and $\beta - J_C$ characteristic plots of IBM 5AM HP. From Figure 33, we can see that the J_C peak is clipped at a lower current density in the case of IBM 5AM HB even at 300K. Also, the J_B rise due to Kirk effect and HBE, which seems to be at the same J_C at which it is clipped, jumps much higher for HB than what is seen for its HP counterpart. The jump also seems to occur at lower J_C for HB than for HP.

The clipping and roll-off J_C's values match closely with the J_C's at which β rolls off and degrades sharply at high injection. Therefore, it may be that $J_{C(Kirk)}$ for the HB device is smaller. To clarify the issue, the slopes of the gummel, i.e. $\frac{d(logJ_C)}{dV_{BE}}$ and $\frac{d(logJ_B)}{dV_1 BE}$ are plotted vs. J_C for three different temperature points in Figures 35, 36, and 37. It can be clearly seen that the $J_{C(Kirk)}$, characterized by the point where $\frac{d(logJ_B)}{dV_{BE}}$ suddenly increases in the slope curves, is 0.2mA/μm^2 at 162K and 0.3mA/μm^2 at 43K. The trend of $J_{C(Kirk)}$ over

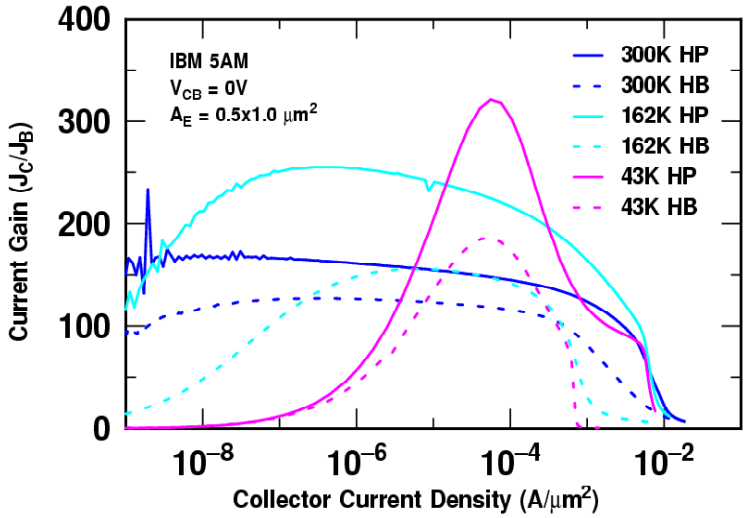

Figure 34: Comparison of Current Gains for IBM 5AM HP and HB at different temperatures.

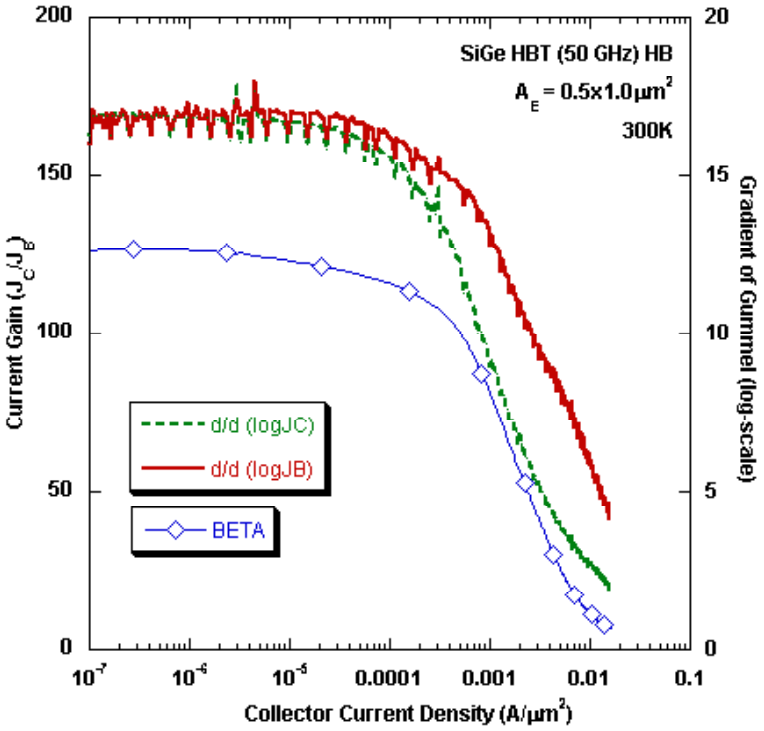

Figure 35: Slope of Gummel Characteristic vs. Collector Current Density for IBM 5AM HB at 150K.

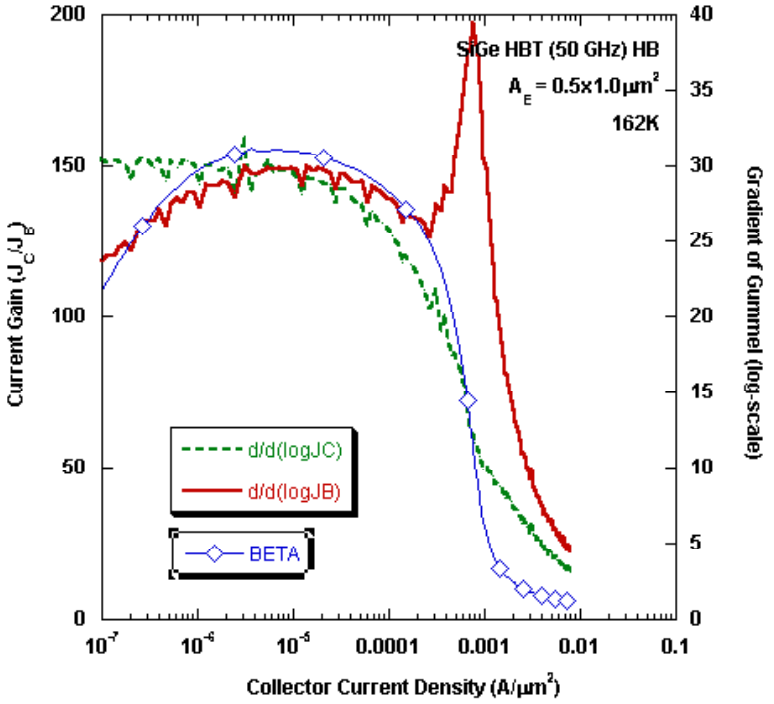

Figure 36: Slope of Gummel Characteristic vs. Collector Current Density for IBM 5AM HB at 162K.

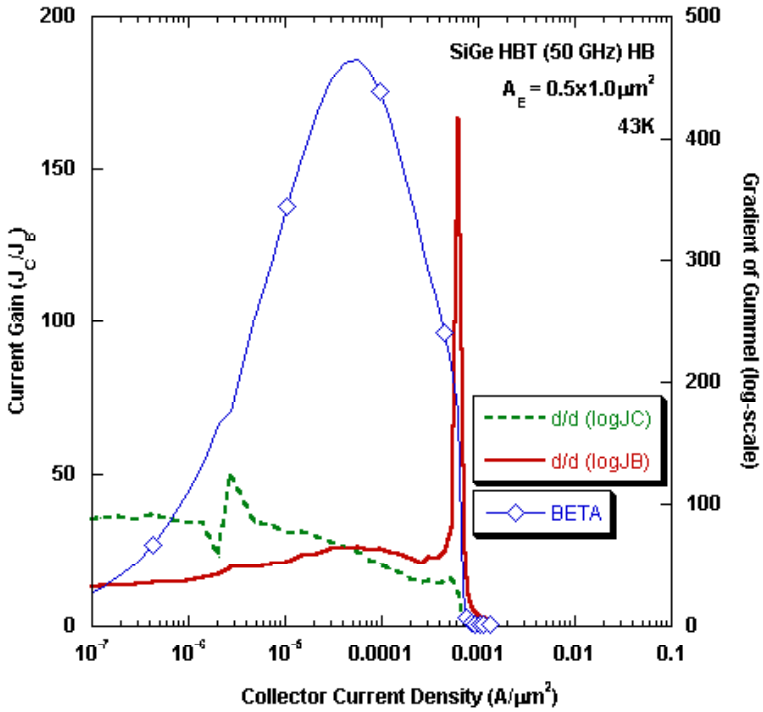

Figure 37: Slope of Gummel Characteristic vs. Collector Current Density for IBM 5AM HB at 43K.

temperature therefore, is common with the HP device, but the values are much lower. This can be explained by the fact that smaller collector doping, N_{dc}, in the HB device, requires less current density to deplete the CB SCR, and thus onset of Kirk effect and HBE shifts to lower injections. It is also noticeable from the slope plots that the magnitude of HBE, as characterized by magnitude of the $\frac{d(logJ_B)}{dV_{BE}}$ jump at $J_{C(Kirk)}$, is negligible at 300K, but gets worse dramatically as temperature decreases. The $\frac{d(logJ_B)}{dV_{BE}}$ jump increases from negligible at 300K to 25/V at 162K to almost 350/V at 43K. The values at 162K and 43K are much larger than what was found in the HP device and the increases over temperature were much less for the HP device as well. This can be explained if the Ge-retrograding scheme is different in the HB device, i.e. the heterojunction barrier might be steeper for the HB device compared to the HP device, which would result in this difference. This concept is discussed in detail in [34], which states that the steeper the retrograde, the worse is the magnitude of HBE, and lower is the $J_{C(Kirk)}$. This suggests that there might be more than just a collector doping variation between these two flavors of first generation technology.

It can be seen from the gummel and the slope plots that the roll-off of J_B due to quasi-saturation of the base is reduced over temperature, not by the fact that intrinsic base resistance drops, but more by the fact that $J_{C(Kirk)}$ is very near the current density where the quasi-saturation starts to occur, and J_B jumps sharply before it can saturate much. Also, since the $\frac{d(logJ_C)}{dV_{BE}}$ can be seen to be quite high at the point that the Kirk effect occurs, in comparison to what was seen in HP, the steepness of the drop of $\frac{d(logJ_B)}{dV_{BE}}$, during HBE, is much higher in the case of HB devices (20 compared to 7 for HP, from Figures 36 and 19, at 162K). This consequently means that the J_C clipping at high injection as can be seen in the gummel characteristic is much more visible for the HB device than for the HP device.

The peak β for the HB devices are also monotonically lower than that for the HP device as is clear from Figure 34. This again suggests that there might be some Ge-profile differences between HP and HB devices.

Both V_A and BV_{CEO} of the HB device should theoretically be better than HP device.

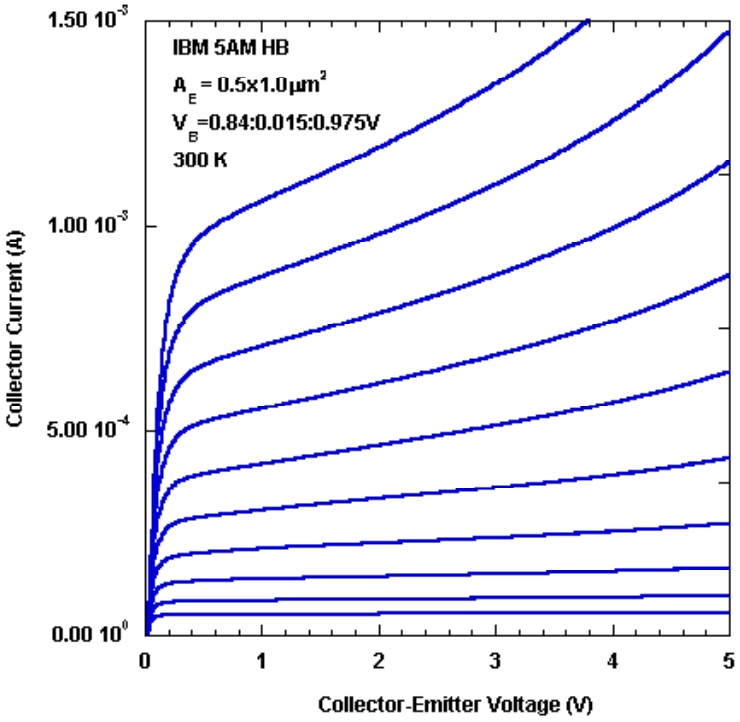

Figure 38: Forced V_{BE} Output Characteristics for IBM 5HB at 300K.

V_A should be higher as HB devices have lower collector doping, which, in turn means that the SCR region width increase will predominately be in the collector region, thereby not affecting W_b, and thus V_A should be more ideal.

The forced-V_{BE} output characteristics can be seen in the following figure.

Similar techniques were used to calculate M-1 and BV_{CEO}, for the HB device, as were used for the HP device. The results are depicted as follows.

The trends of V_A and BV_{CEO} with temperature were common to what was seen in HP, and the values were higher, as predicted.

The forced-I_B output characteristic plots at high-injection are presented in Figures 42-44.

It can be seen from both the forced-V_{BE} and the forced-I_B output characteristics that at high-injections, the collector current's rise with V_{CE} is generally higher (especially for the forced I_B case) than what was seen in HP (Figures 28, 29, 30, 22, and 23). But as V_A is

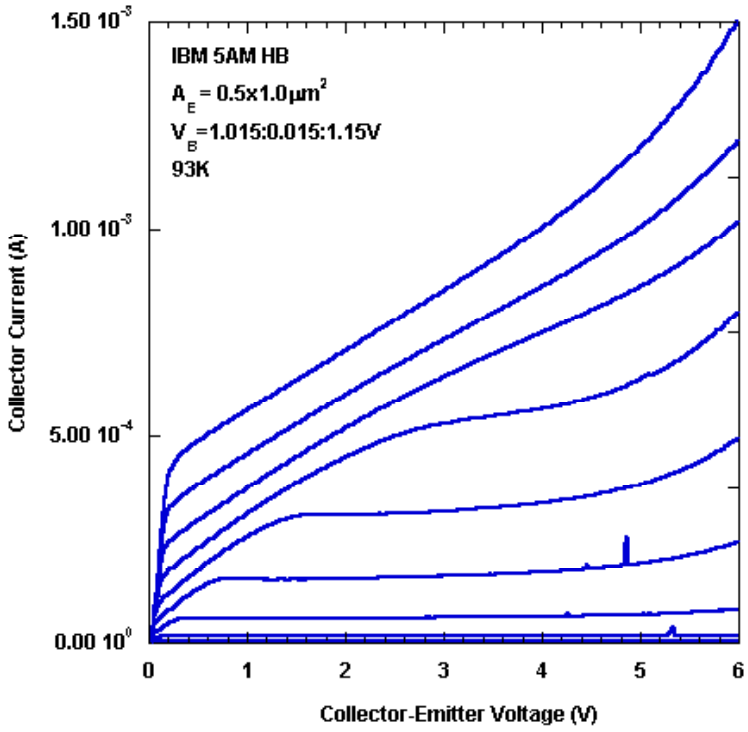

Figure 39: Forced V_{BE} Output Characteristics for IBM 5HB at 93K.

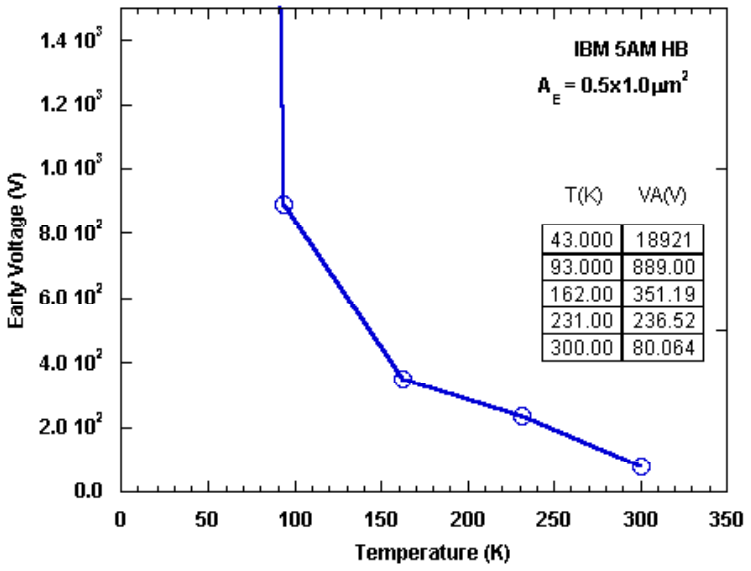

Figure 40: Variation of Early Voltage with temperature for IBM 5AM HB Technology.

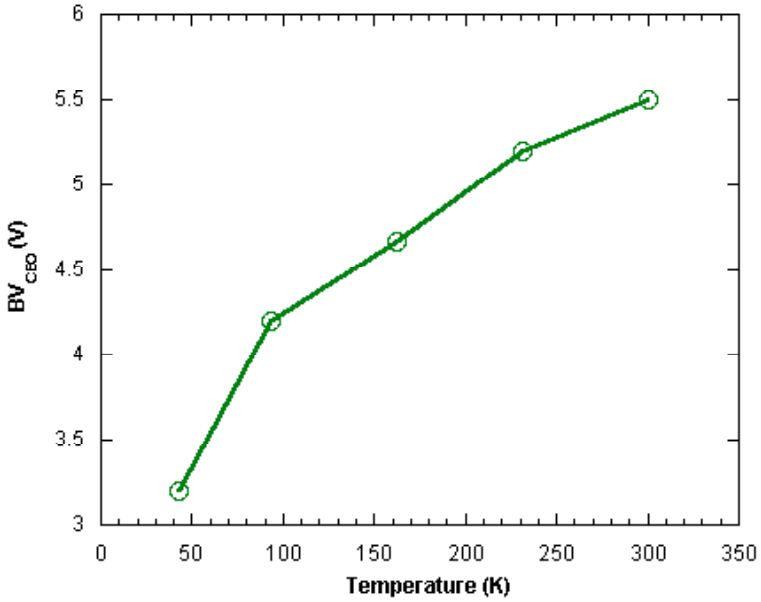

Figure 41: Variation of BV_{CEO} with temperature for IBM 5AM HB Technology.

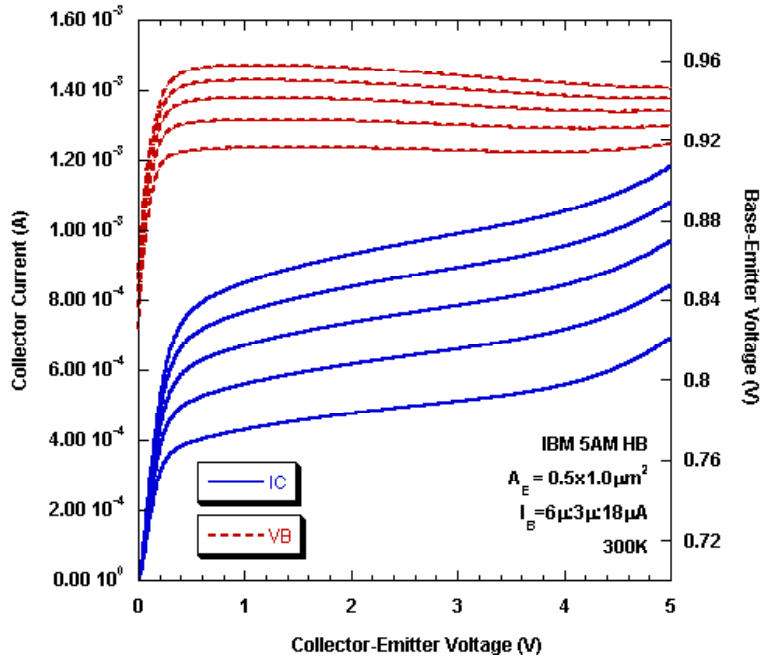

Figure 42: Forced I_B Output Characteristics for IBM 5AM HB at 300K.

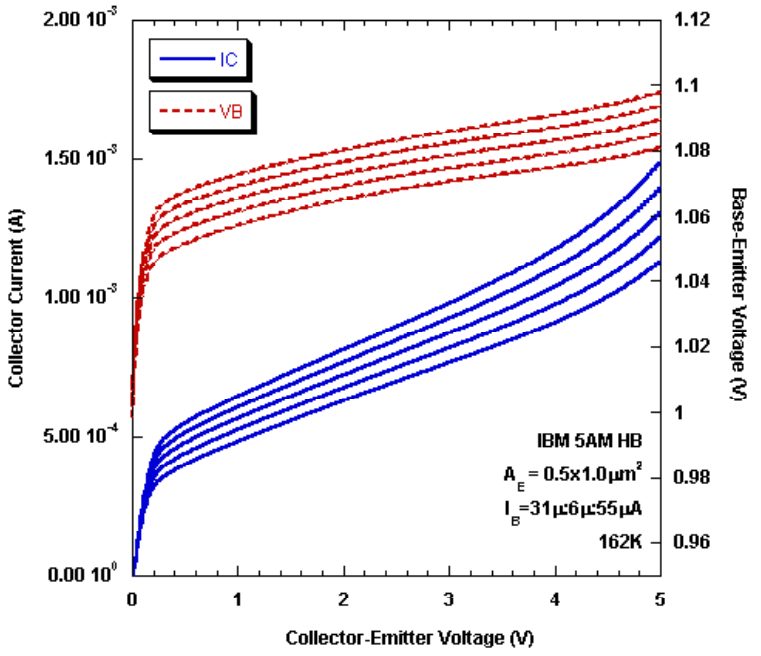

Figure 43: Forced I_B Output Characteristics for IBM 5AM HB at 162K.

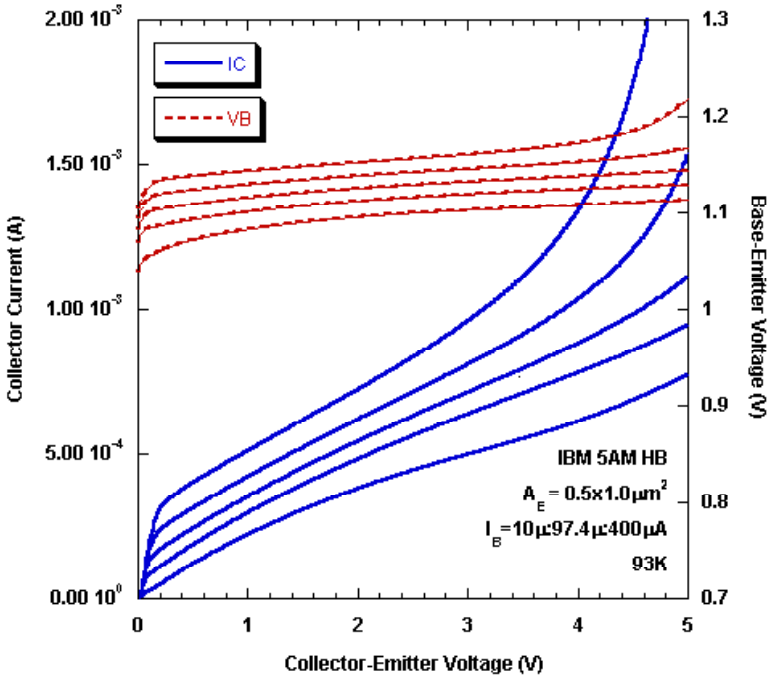

Figure 44: Forced I_B Output Characteristics for IBM 5AM HB at 43K.

higher for HB devices, we know that the trend is opposite at low injections. Also, it can be seen that though V_{BE} for 300K (Figure 42 follows the same downward trend with V_{CE} as seen in the HP case in Figure 28, the characteristics at 162K and 43K do not follow the same trend. These effects can be attributed to many factors working together and against each other, for example self-heating, HBE, and neutral-base-recombination (NBR), discussed in detail in [3] and [6]. We know that self-heating is decreased at low temperatures, NBR is increased, [3]. If NBR is higher for the HB device, it can explain the opposite trend of V_{BE} at lower temperatures, where self-heating is weakened, NBR is the dominant force, which increases I_B at low V_{CE}s more than higher temperatures, but decreases in strength as V_{CE} increases and the W_b decreases, so effective I_B decreases, and V_{BE} rises with V_{CE} to maintain the constant I_B.

The NDR hillocks that were seen forming at the edge of quasi-saturation for the high performance device in its forced-V_BE output characteristic (Figure 23) becomes less pronounced, if not totally disappears, for the high breakdown device. The forced-I_B does not show any NDR trends at low currents or high injections either.

2.3.4 Profile Design and Optimization

In order to reduce the effect of base tunneling, which depends on the emitter doping at the EB junction, a lower doped epitaxial emitter-cap region can be deposited over the SiGe base [33]. Also, since the Kirk effect at lower temperatures are shifted to higher injection regions, the collector can be doped lightly and ramped upward to the highly doped subcollector to reduce deep collector freeze-out [34]. This lighter doping at the CB junction will increase BV_{CEO}.

2.4 Summary

It is important to know the static characteristics of SiGe HBTs and how they vary with temperature before they are used in circuits for cryogenic applications. The characteristics

also help in understanding the device physics behind the numerous thermally activated parameters of the SiGe HBT.

In this chapter, the theory of how SiGe HBT *dc* performance might vary with temperature was presented followed by verification of the concepts with results and discussion. We saw that there are four distinct regions of the low temperature gummel and β plots, (i) very low injection, where base and collector tunneling occurs, (ii) low injection, where peak β is reached, (iii) medium injection, where β starts to roll off due to Ge-grading effect, and (iv) high injection, where Kirk effect and HBE occur. We saw in detail how current and gain are affected in all these regions over temperature. We also saw how Early voltage, resistances, and breakdown characteristic of the 5AM device changes with temperature. We can conclude that the theory predicts and explains the experimental findings, and as certain figure of merits improve with low temperature, such as $\beta \cdot V_A$, others degrade, such as breakdown and operating regime.

To further investigate this tradeoff, this chapter compared the *dc* performance of a High Performance device with that of High Breakdown device. The differences between HP and HB were expected, however, certain differences suggested that there might be more than just a collector doping difference between the two flavors of the same technology. Finally, these insights were used to suggest some possible profile optimizations for devices optimized for cryogenic performances.

CHAPTER III

IMPLICATIONS OF TECHNOLOGY SCALING ON CRYOGENIC STATIC PERFORMANCE OF SIGE HBTS

3.1 Introduction

Technology scaling, or alteration of generation, is accompanied by changes in various device parameters through the alteration of key technology parameters, such as the base width, W_b, Ge profile, and doping profiles. These changes in the device technology are usually aimed towards optimizing the SiGe HBT to better meet the requirements of the industry at the time of design. Also, the devices are usually not optimized for low temperature. Therefore, in addition to understanding what effects low temperature might have on these different technologies for cryogenic circuit applications, it is important to know how these effects differ. Also, their comparison, especially at low temperatures, may unearth the implications of a lot of the changes that are made during technology scaling, as we know, that many effects are accentuated by low temperature. This will help further arm device designers the knowledge to make more educated device designs and optimizations in the future, and circuit designer, to best utilize the technology.

This chapter will present the *dc* characterization results and discussion for IBM's second generation high performance (IBM 7HP), third generation high performance (8HP), and fourth generation high breakdown (IBM 9HB) SiGe HBTs. The comparison of IBM 5AM HP with IBM 7HP, IBM 8HP, and IBM 9HB, should illustrate the effects of technology generation scaling. Also, since the exact doping, and Ge profiles are not known for any of the more recent technologies, this chapter will make a reasonable effort to explain

the reason behind some of the observed phenomenon.

3.2 Background

3.2.1 Description of Technology

Table 1 in Chapter 1 shows the representative SiGe HBT parameters for first, second, third and fourth generation technologies. It can be seen that the width is monotonically decreased with progress of generations, and *dc* characteristic-wise, peak β and V_A is increased while breakdown voltage parameters are worsened. The table shows the High Performance flavor of each generation, and it can be stated with reasonable certainty that the high breakdown flavor of each will have higher breakdown parameters and lower β and V_A, achieved through higher collector doping.

As base width decreases over generations, it can be safely assumed that the peak Ge content in the base is also increased, maintaining the same level of stability [34]. The grading would probably increase as well. The fourth generation device has a higher reported β, than that which was reported for the third generation High Performance device, but has the same W_E. Also, the breakdown parameters of IBM 9HP are very similar to that for the third generation High Performance device, which may mean that, the collector doping is almost the same for the last two generations. This study will deal with the high breakdown flavor of IBM 9T, which may have a lower collector doping than the IBM 8HP. The exact profiles are proprietary to IBM and are not disclosed, but the doping profile presented in Figure **??** in Chapter 1, is representative of an IBM 5HP technology, which has a near 10% trapezoidal Ge profile. The Technology Scaling section in Chapter 1 gives more insight into these four generations. The reader can also refer to [20], [21], [22], and [24] for more information.

3.2.2 Experimental Setup

The devices that were measured in this experiment were IBM 7HP 0.28x2.5μm^2, IBM 8HP 0.2x2.5μm^2, and IBM 9HB 0.12x2.5μm^2. The devices were collected from on-wafer,

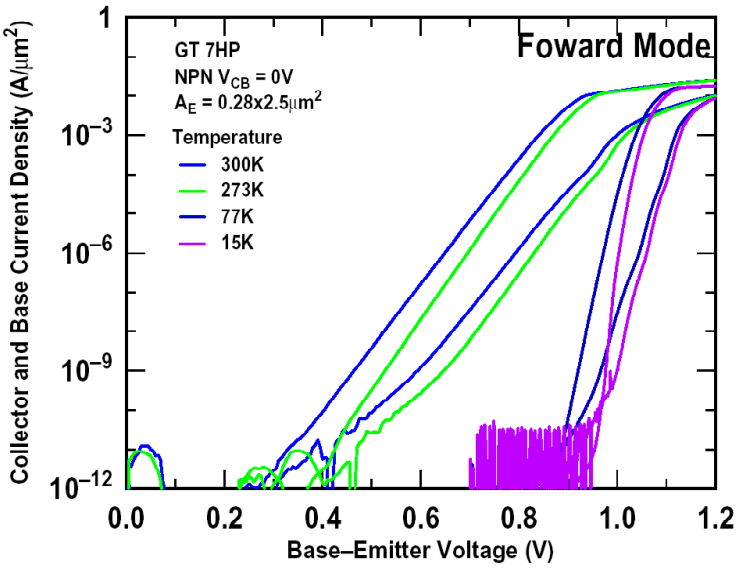

Figure 45: Gummel Characteristic of IBM 7HP at different temperatures.

diced, packaged, just like what was done for the IBM 5AM devices described in Chapter II, and then the package was inserted into the cryostat-4155 setup shown in Figure **??**. Ten temperature points were selected including, 15K, 30K, 50K, 77K, 90K, 120K, 150K, 210K, 273K, and 300K and *dc* characterization was done at all these points.

3.3 Results and Discussion

3.3.1 Second Generation SiGe HBT Static Characteristics

For IBM 7HP, the gummel characteristic and $\beta - J_C$ plots over temperature are presented in Figures 45 and 46.

Carrying on the same analysis as was done for IBM 5AM HP and HB devices in Chapter II, it can be seen that the temperature trends, including current, gain, built-in voltage, transconductance, Ge-grading effects, and tunneling effects, are similar to what was seen in IBM 5AM devices. The J_C gummel can be seen to roll off starting at a J_C of around 0.1mA/μm^2, which is higher than what was noticed for the IBM 5AM HP devices, which rolled off around 0.01mA/μm^2, Figure 16. This roll-off is at medium injection and coincides well with the J_C at which peak β occurs. The roll-off can be chiefly attributed to

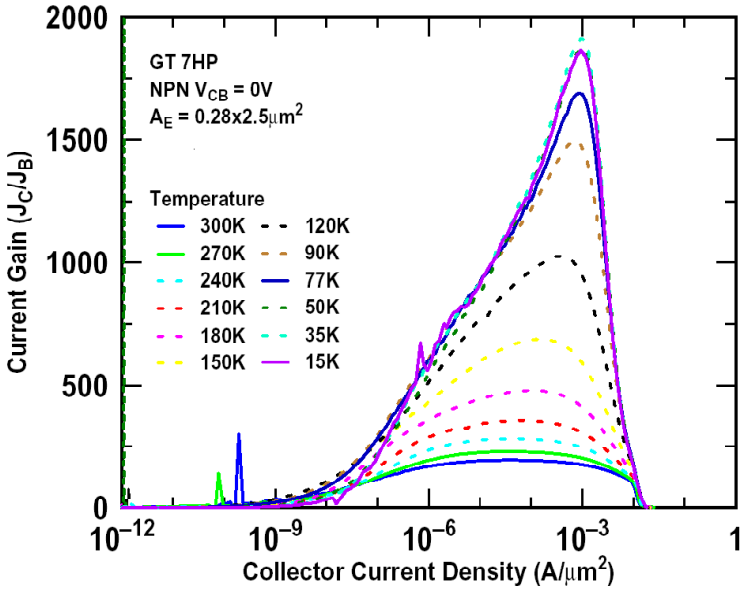

Figure 46: Current Gain for IBM 7HP at different temperatures.

Ge-grading effect, as can be proven to be so by looking at the J_C and J_B gummel slope plots, which plots $\frac{d(logJ_C)}{dV_{BE}}$ and $\frac{d(logJ_B)}{dV_{BE}}$ vs. J_C, Figure 47 at 300K. It can be clearly seen that at the roll-off, $\frac{d(logJ_C)}{dV_{BE}}$ decreases more than $\frac{d(logJ_C)}{dV_{BE}}$ and therefore proves that the roll-off is due to Ge-grading, which primarily affects J_C, just like in IBM 5AM. At high injection, $\frac{d(logJ_C)}{dV_{BE}}$ drops as $\frac{d(logJ_B)}{dV_{BE}}$ jumps in Figure 47 showing the onset of Kirk effect and HBE. The $J_{C(Kirk)}$ can be seen to rise from 5mA/μm^2 to 7mA/μm^2 to 9mA/μm^2 as temperature falls from 300K to 150K to 50K (Figures 48 and 49). The trend of $J_{C(Kirk)}$ rising with falling temperature resembles that seen in IBM 5AM technology but the values are larger than that IBM of 5AM HP and HB $J_{C(Kirk)}$. This can be attributed to the fact that the collector doping in IBM 7HP is higher. This assumption can be backed up by the fact that the reported BV_{CEO}, [21], for the technology is lower than that of IBM 5AM, which is another effect of increased collector doping.

The magnitude of the HBE that occurs at $J_{C(Kirk)}$ can be measured from the change in slope of $\frac{d(logJ_B)}{dV_{BE}}$ from the slope curves and is found to change from 5/V to 16/V to 20/V as temperature decreases from 300K to 150K to 50K. This trend is also not out of the norm but

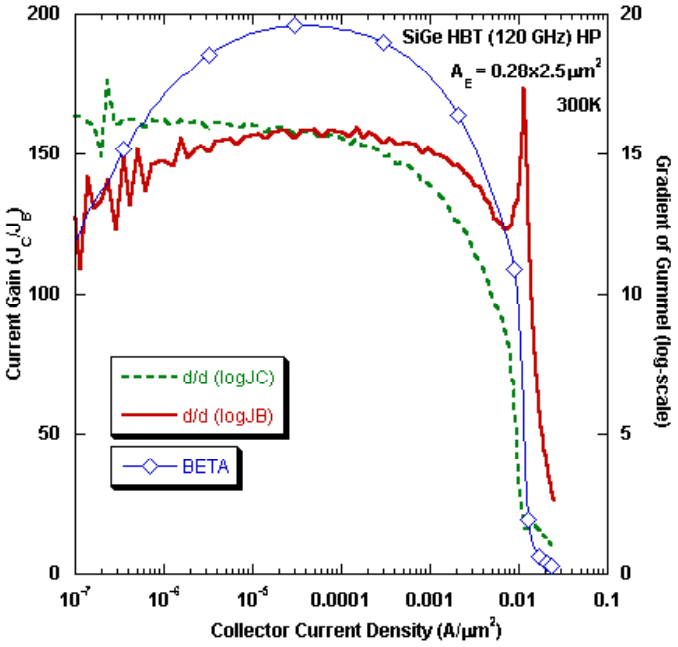

Figure 47: Slope of Gummel Characteristic vs. Collector Current Density for IBM 7HP at 300K.

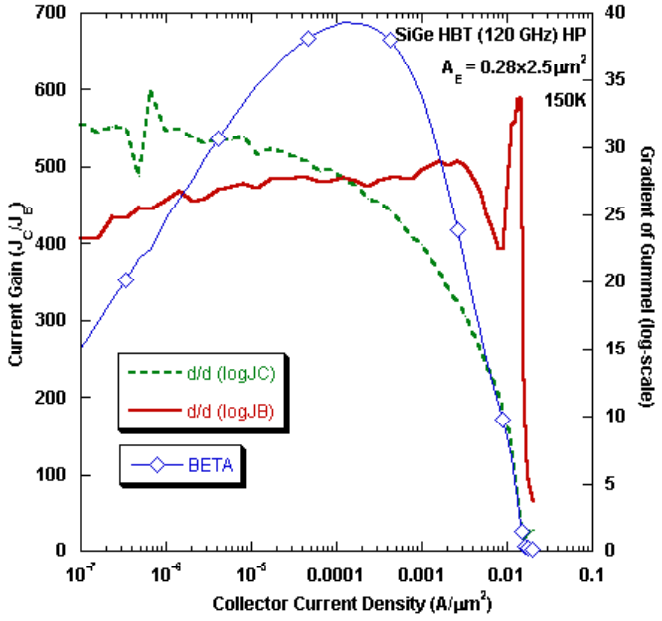

Figure 48: Slope of Gummel Characteristic vs. Collector Current Density for IBM 7HP at 150K.

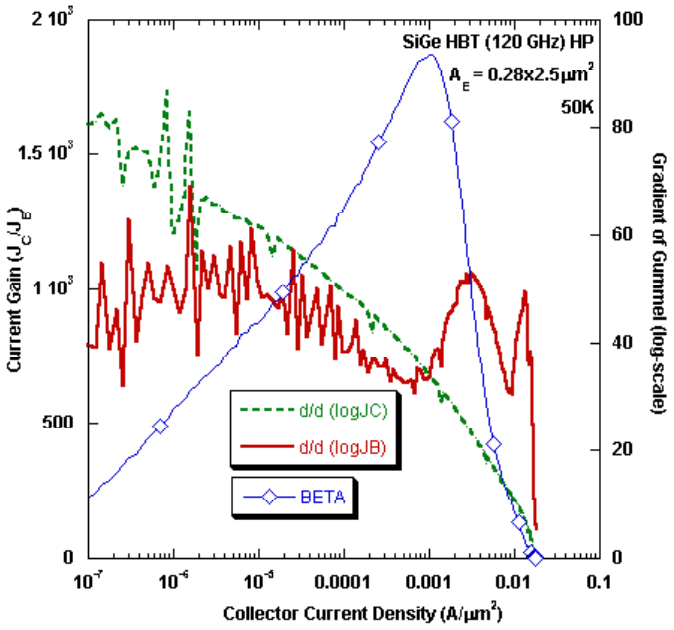

Figure 49: Slope of Gummel Characteristic vs. Collector Current Density for IBM 7HP at 50K.

the magnitudes are monotonically less than that which was observed in IBM 5AM HP and HB, and can be explained by the Ge profile difference, in terms of retrograding, between 5AM and 7HP, which was discussed in an earlier section [34].

Before $J_{C(Kirk)}$ is reached, the J_B roll-off, denoted by drop in $\frac{d(logJ_B)}{dV_{BE}}$ from its peak, due to quasi-saturation is not much. This can be noticed clearly if Figure 48 is compared against Figure 19 at 162K. The roll-off due to quasi-saturation is reminiscent of the case in IBM 5AM HB. The $\frac{d(logJ_B)}{dV_{BE}}$ at the onset of Kirk effect can be read to be around 15/V for IBM 7HP at 162K (Figure47) as opposed to just 5/V for IBM 5AM HP at 162K (Figure19), i.e. the $\frac{d(logJ_B)}{dV_{BE}}$ drop is significantly higher at Kirk effect for IBM 7HP and the clipping is more severe and can be clearly seen in the gummel plot in Figure 45. The explanation for the weak J_B roll-off at current densities right before onset of Kirk effect, due to quasi-saturation, can be explained by the fact that the base resistance is lower for IBM 7HP compared to that for IBM 5AM and not because of $J_{C(Kirk)}$ occurring at low current densities, which was the case for IBM 5AM HB.

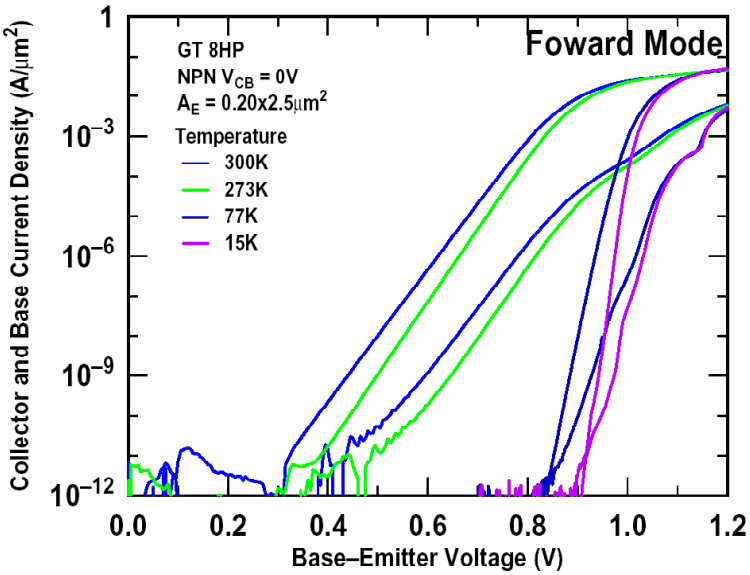

Figure 50: Gummel Characteristic for IBM 8HP at different temperatures.

3.3.2 Third Generation SiGe HBT Static Characteristics

The gummel and $\beta - J_C$ characteristics for the IBM 8HP 0.2x2.5μm^2 can be seen in Figures 50 and 51.

As can be seen, the effect of temperature on the current, gain, transconductance, built-in voltage, Ge-grading, and tunneling effect characteristics are very similar to what was seen in IBM 7HP, except that the roll-off for J_C starts at a higher current density, and at a higher bias voltage, V_{BE}. Also, from the gummel and the gain characteristic, it is clear that the J_B roll-off due to quasi-saturation is more prominent for IBM 8HP resembling what was seen in IBM 5AM HP, rather than IBM 7HP. This means that certain parts of the base in IBM 8HP device may have higher resistance than those in IBM 7HP, and may be due to the effective dopant concentration being less than that in 7HP.

From the slope curves, Figures 52, 53, and 54, the J_C slope level, $\frac{d(logJ_C)}{dV_{BE}}$, at the onset of Kirk effect, are less than 5/V at all temperature points, as opposed to the higher $\frac{d(logJ_C)}{dV_{BE}}$ in the case of IBM 7HP. This means that J_C does not clip as sharply as it did for IBM 7HP and IBM 5AM HB, and this is obviously seen when IBM 8HP gummel, Figure 50, is compared

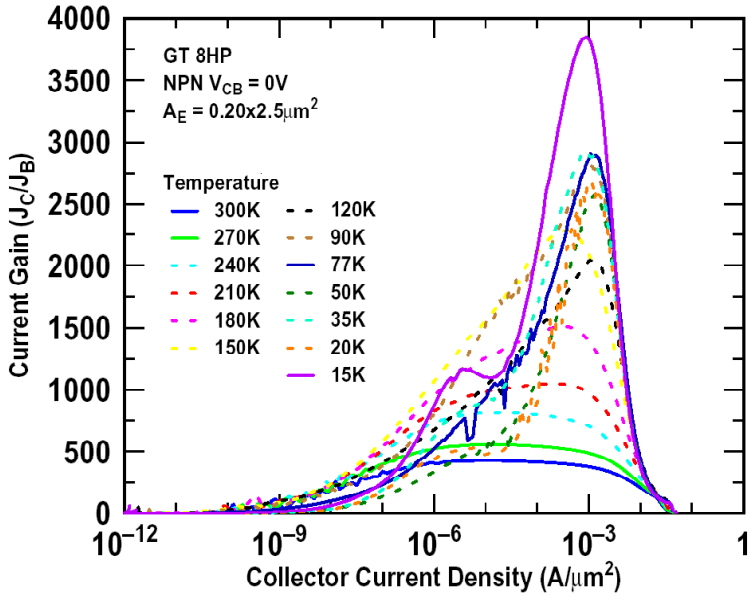

Figure 51: Current Gain for IBM 8HP at different temperatures.

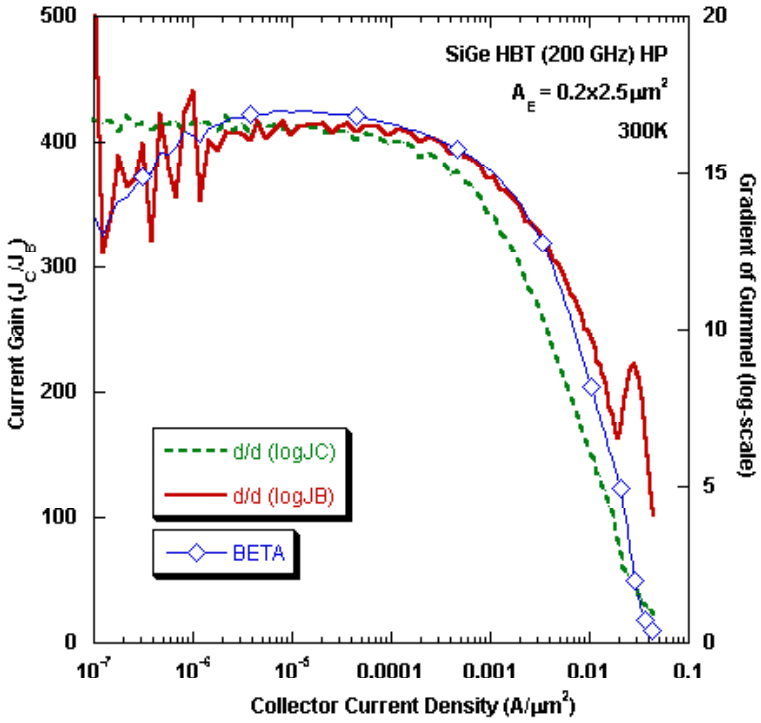

Figure 52: Slope of Gummel Characteristic vs. Collector Current Density for IBM 8HP at 300K.

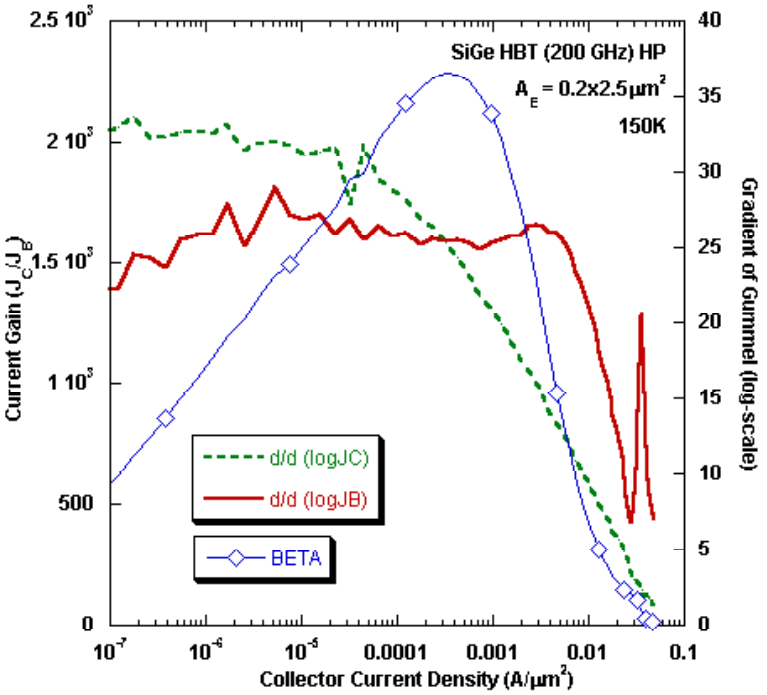

Figure 53: Slope of Gummel Characteristic vs. Collector Current Density for IBM 8HP at 150K.

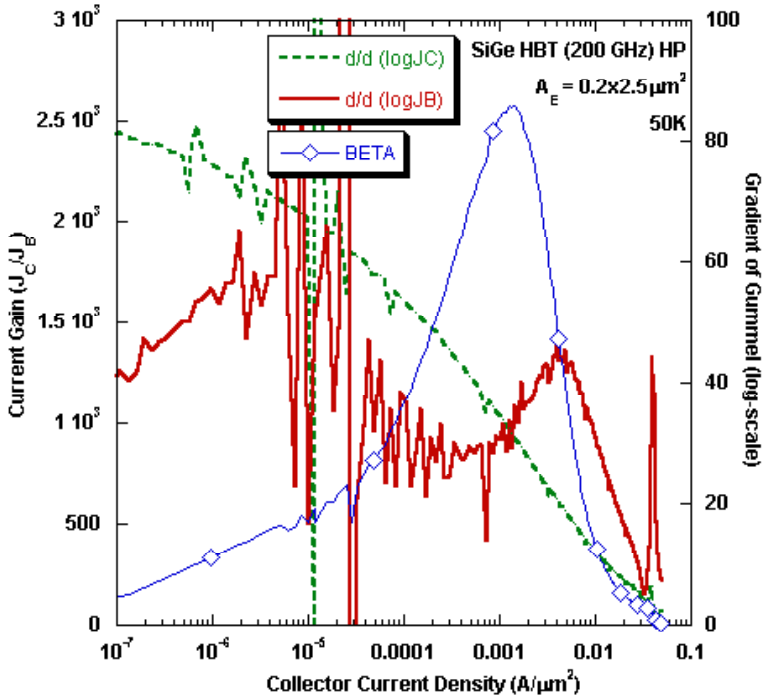

Figure 54: Slope of Gummel Characteristic vs. Collector Current Density for IBM 8HP at 50K.

with IBM 7HP gummel (Figure 45), at high injections.

The $J_{C(Kirk)}$ values, derived from the J_C and J_B slope plots, for IBM 8HP followed the same trend as IBM 7HP and IBM 5AM over temperature, increasing from 15 mA/μm^2 to 20 mA/μm^2 to 35 mA/μm^2 as temperature drops from 300K to 150K to 50K. These values are much higher than what was seen for IBM 7HP, and IBM 5AM. This can be attributed to an increase in collector doping coupled with a modified Ge-retrograding scheme deep in the collector. The magnitude of the HBE effect, as seen by the jump in $\frac{d(logJ_C)}{dV_{BE}}$, from the slope curves, Figures 52, 53, and 54, increased from 2/V at 300K to 13/V at 150K to 35/V at 50K, following the norm. Each magnitude was less than what was seen in IBM 7HP, and can be explained again by a difference in retrograding of the Ge-profile in the collector. A flatter retrograde which reaches inside the collector for IBM 8HP, which takes the edge of the obviously higher peak Ge content will make sense and explain the discrepancy between IBM 7 and 8HP.

The *dc* results shown for IBM 8HP match well with what was shown in [44], where the similar technology was characterized at low temperatures.

3.3.3 Fourth Generation SiGe HBT Static Characteristics

The gummel (collector current and base currents plotted separately for clarity), and gain characteristic plots for IBM 9HB 0.12x2.5μm^2 are presented in the following figures.

Similar trends with temperature are seen for current densities, gain, transconductance, built-in voltage Ge grading, and tunneling, to the previously discussed devices. However, the J_C roll-off at medium injection is seen to be higher for IBM 9HB compared to IBM 8HP, IBM 7HP, and IBM 5AM. The $J_{C(Kirk)}$ rises from 10 to 15 to 20 mA/μm^2 (from the slope curves, Figures 58, 59, and 60, as temperature is dropped from 300 to 150 to 50K. The magnitudes are higher than those seen for IBM 7HP, and IBM 5AM, but lower than those seen for IBM 8HP.

This anomaly can be explained by the fact that this technology is the High Breakdown

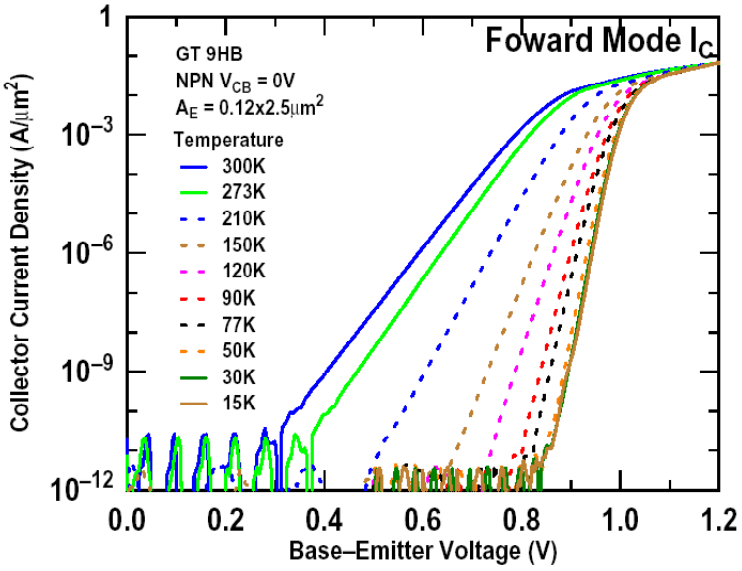

Figure 55: Forward Mode Collector Current Density for IBM 9HB at different temperatures.

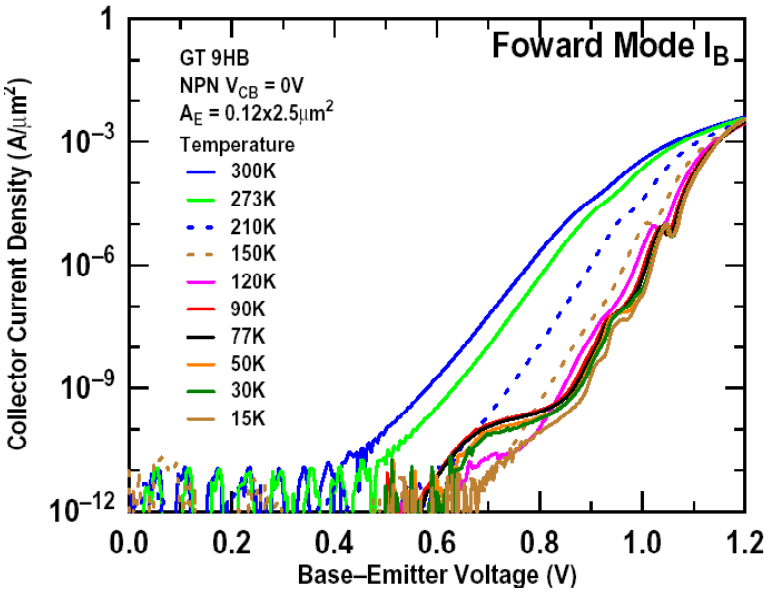

Figure 56: Forward Mode Base Current Density for IBM 9HB at different temperatures.

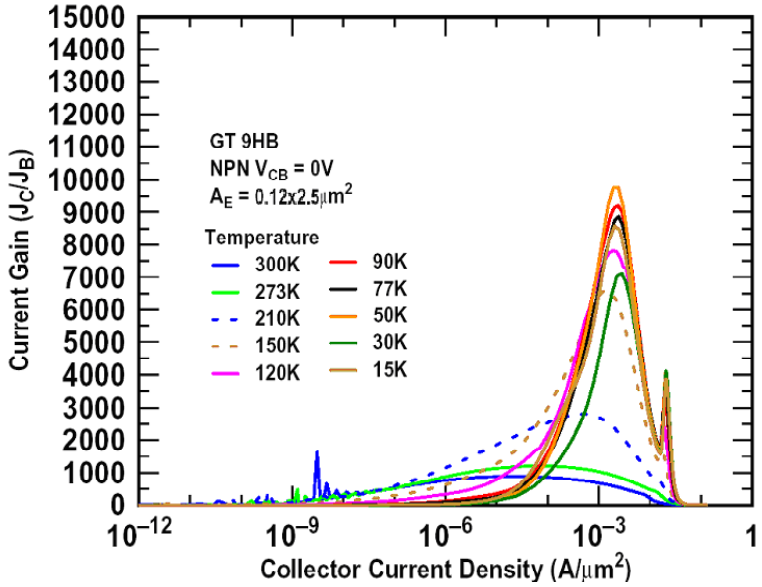

Figure 57: Current Gain for IBM 9HB at different temperatures.

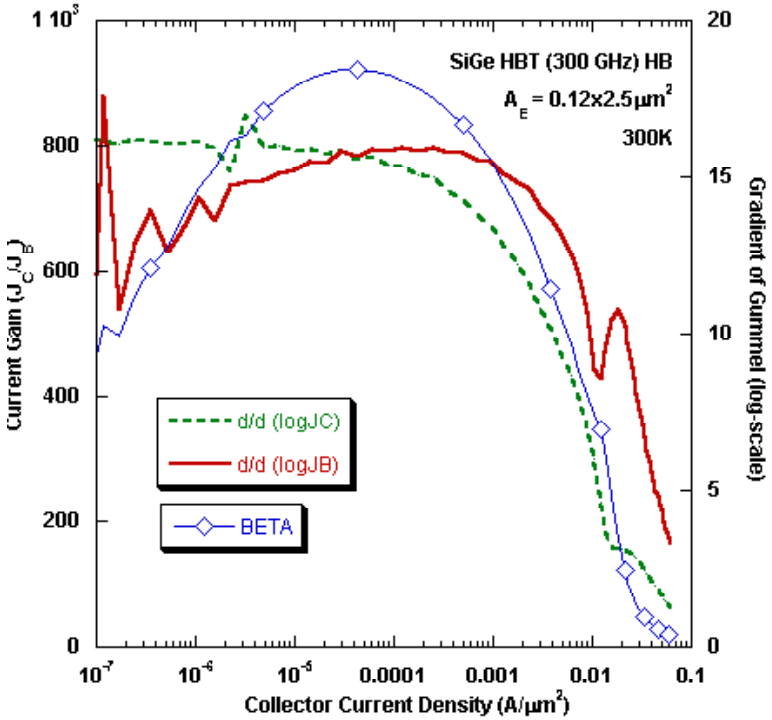

Figure 58: Slope of Gummel Characteristic vs. Collector Current Density for IBM 9HB at 300K.

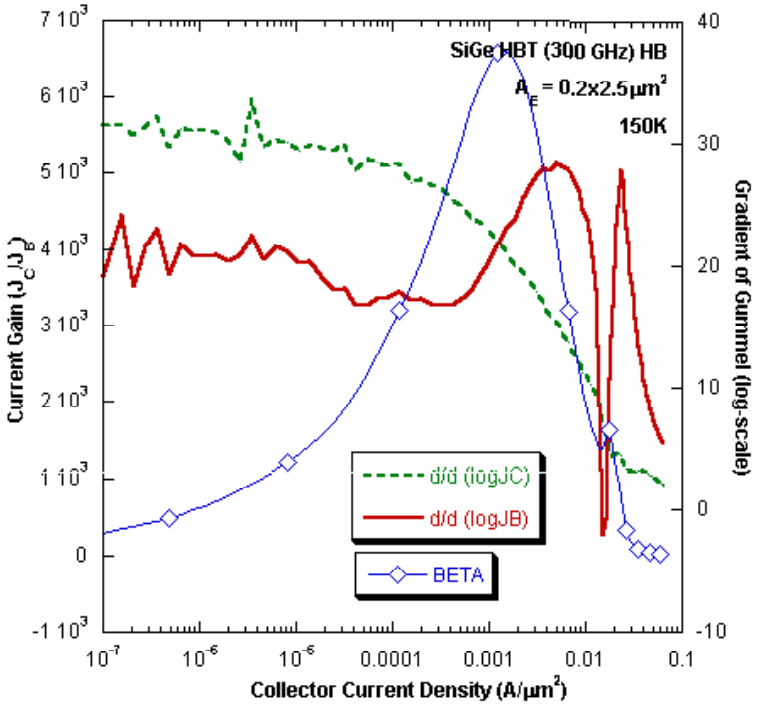

Figure 59: Slope of Gummel Characteristic vs. Collector Current Density for IBM 9HB at 150K.

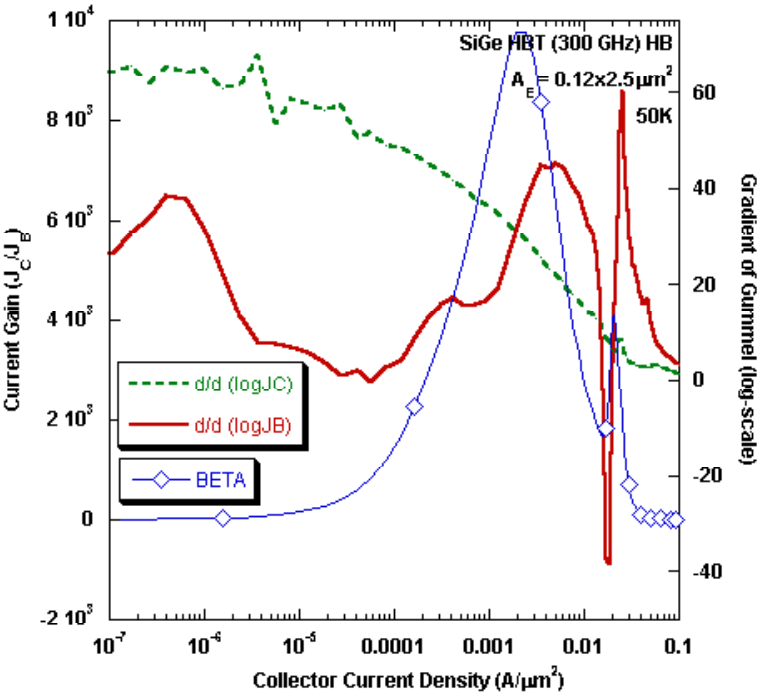

Figure 60: Slope of Gummel Characteristic vs. Collector Current Density for IBM 9HB at 50K.

flavor of the fourth generation technology, so it must have higher collector doping, as was predicted above, to improve its breakdown parameters, consequently making the $JC(Kirk)$ smaller. The magnitude of HBE, as derived from the slope plots from the $\frac{d(logJ_B)}{dV_{BE}}$ rise, is seen to change from 2/V at 300K to 30/V at 150K to 80/V at 50K. These values are higher then those seen for 7HP and 8HP, are comparable to those in 5AM HP, and are better than those seen in 5AM HB.

For the IBM 9HB devices, there exists an anomaly in the gummel characteristic that is non-existent in the other technologies. In the forward mode, the base current actually drops to lower values before it jumps due to HBE effect right before the Kirk effect occurs. This is clearly seen in the forward mode J_B plots in Figure 56 and and in the negative slope, $\frac{d(logJ_B)}{dV_{BE}}$ values reached in the slope curves (Figures 58 - 60). This behavior is peculiar to IBM 9HB and can also be attributed to be an NDR as base current slope with respect to V_{BE} becomes negative. The effect becomes more prominent as temperature drops, just like the NDR in the output characteristic for IBM 5AM HP (Figure 23). Therefore, it is only natural to guess that they may be related. The discussion in [45] observes these base 'dips' to be stronger in aggressively scaled technologies like IBM 9T, therefore, the data agrees in both the studies in that respect.

For further comparison between the static characteristic of the technologies and their variation, in order to visualize the differences in peak β, peak J_C, J_C roll-off current levels, and V_{BE} bias levels, it is important to look at the overlay of plots of all technologies. The following figures overlay the gummel and gain characteristics over temperature for all the four generations of technology.

It can be clearly noted that the peak β, from Figure 62 and 63, increases with technology generation, and occurs at higher J_Cs. This can be explained from the gummel characteristic plots, which show a monotonic increase in J_C at the same temperature points for more recent technologies.

From Figure 61, it is clear that J_B levels for the second, third and fourth generation

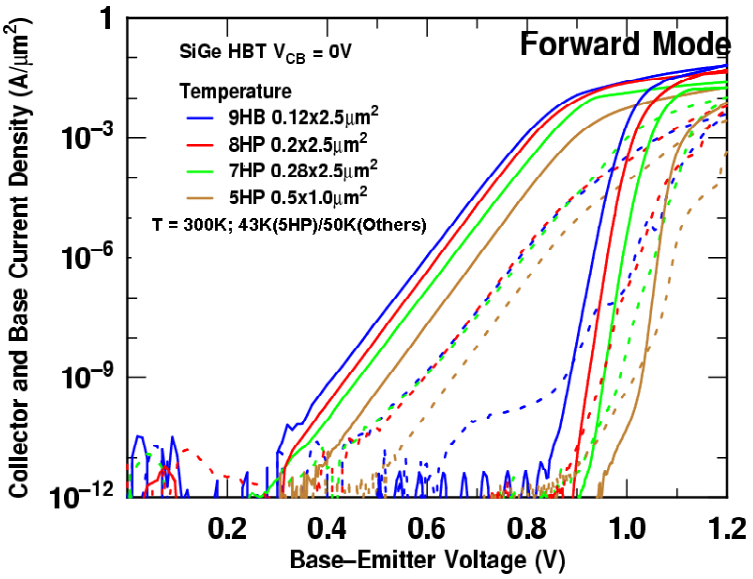

Figure 61: Gummel Characteristic for all four technology generations at 300K and 43K.

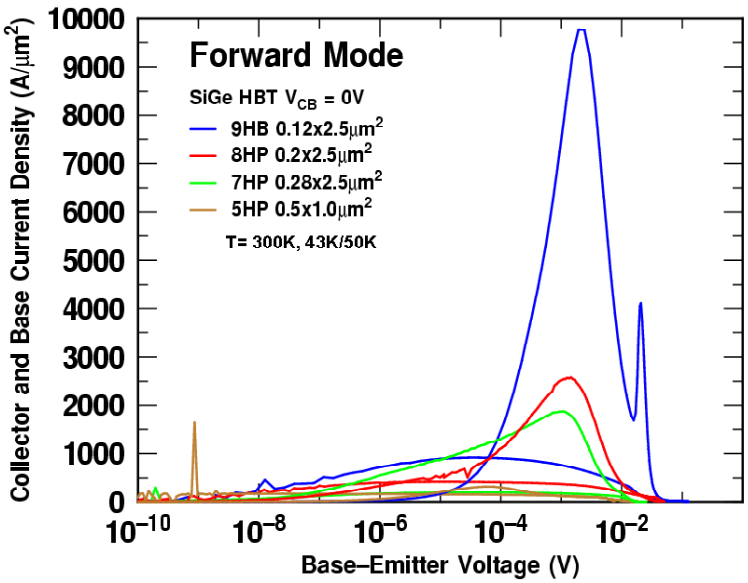

Figure 62: Current Gain for all four technology generations over temperature.

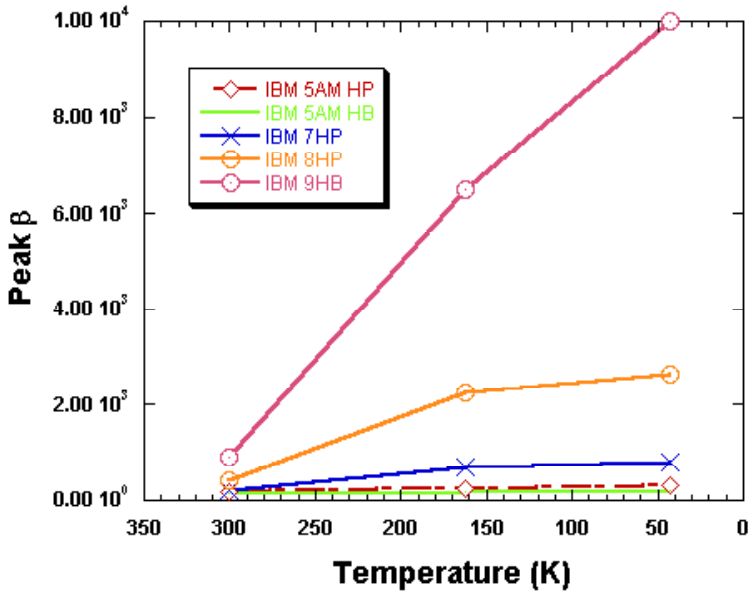

Figure 63: Peak Current Gain for all four technology generations over temperature.

technologies are comparable, even for low temperatures, but that fof IBM 5AM is much lower, which suggests that the base doping level for IBM 5AM is much lower than that for IBM 7HP, IBM 8HP, and IBM 9HB. Comparing the J_Bs in the gummel plot over temperature, it is clear that at low temperatures, the base currents become quite non-ideal at very low and low injections. This effect is worsened with technology generation, and IBM 9HB has the most undulated base current, reflected in its β characteristic plot, Figure 57 by the presence of more than one peak at lower temperatures. The Ge-grading effect, which determines the roll-off at medium injection levels, definitely increases in magnitude at lower temperatures, but it is also seen to increase in magnitude over technology generation. The Ge-grading effect can be said to have higher magnitude, if the current gain roll-off steepness increases at medium injection. From Figure 62, this becomes clear. This can be explained by the fact that with technology generation, the peak Ge-content rises in the increasingly narrower base, meaning the Ge-grading at the EB junction rises and therefore, so does the Ge-grading effect.

3.3.4 Summary

In this chapter, the technology scaling effects on cryogenic static characteristics of SiGe HBTs were explored. Four generations of IBM SiGe HBT CMOS technology were compared with each other and some assumptions about the doping and Ge profiles in the transistors were explored.

It was seen that there were many common temperature trends across all technologies, including increase in current gain, built-in voltage, transconductance, Ge-grading effect magnitude, tunneling effect worsening, $J_{C(Kirk)}$, and HBE magnitude, with a decrease in temperature. With technology generation, there was generally an increase in peak J_C, peak J_B (note IBM 7HP, 8HP, and 9HB had almost identical base currents much higher than IBM 5HP), β, $J_{C(Kirk)}$ (except for IBM 9HB, which was < that for IBM 8HP) and Ge-grading effect worsening. Also there was a general decrease in magnitude of HBE (except for IBM 9HB, which had more than IBM 8HP) and built-in voltage. The High Breakdown devices generally had worse HBE magnitudes, lower $J_{C(Kirk)}$s, and lower β than expected. IBM 9HB seemed to have lesser collector doping than IBM 8HP and the base resistance seemed to vary between the different technologies, with IBM 7HP predicted to have the least. These counter-intuitive variations exist side-by-side with the general trends and is very important to understand completely if proper optimization of these technologies is to be achieved.

CHAPTER IV

CONCLUSION

4.1 Conclusion

The thesis provided a comprehensive look at the *dc* performance parameters for all four generations of technology available from IBM, and described how they vary with varying temperatures from room temperature to temperatures below Liquid Nitrogen temperatures. Chapter I introduced the reader to the SiGe HBT BiCMOS technology and showed how the device works and what are the advantages of using such a device over its contenders for high frequency applications.

Chapter II showed the reader what effects might occur at low temperatures to SiGe HBT BiCMOS technology theoretically, and then proved them using experimental data gathered by measuring the IBM 5AM HP technology. IBM 5AM HB technology data was also shown in this chapter, and the comparison between the two technology flavors emphasized the very important tradeoff between gain and breakdown voltage. A detailed analysis was done on the gummel and the current gain plots, which solidified the device level concepts developed earlier in the chapter.

Chapter III presented data from the measurement of state of the art technologies, including IBM 9HB, IBM0 8HP, and IBM 7HP. No such comparison has been done to the author's knowledge, and this comparison showed that although some parameters monotonically degrade or improve over technologies, there are others that vacillate, and there are nuances to the tradeoffs that become apparent at low temperatures, that can be utilized by device designers to optimize SiGe HBTs for low temperature operation.

4.2 Future Directions

Operation in low temperature regimes bring out various non-idealities in SiGe HBT devices. For example, tunneling, HBE, and so on. One such non-ideality which was glossed over while discussing the low temperature forced-V_{BE} curves for IBM 5AM HP, Figures 23, was the NDR effect. Also, the base "dips" as seen for IBM 9HB at high injections in Figure 56, could not be properly explained. The the data to some extent follows [45] but also disproves it in other aspects. Therefore, there is no good answer for this non-ideality problem. Also, since this event occurs in the vicinity of where most circuit designers bias their transistors, if not modeled properly, it can give lots of reliability problems, especially if the circuits are meant for space or other extreme environments, as the NDR is accentuated at lower temperatures. So this poses an interesting problem and may act as one of the future directions for this study, as this can turn out to be a nightmare for circuit designers if not modeled correctly by device engineers, or it can become an enabler of creative circuits, if utilized properly.

This work has done a comprehensive comparative analysis between the high breakdown and high performance flavors of IBM 5AM using gummel and output characteristics but for the more state of the art technologies, IBM 7HP-9HB, the discussion was limited to gummel characteristics and parameters extracted from that. Therefore there is room for exploring the *dc* characterization space in these exciting technologies at low temperatures which will allow us to first identify such problems as NDRm and then solve them. Aside from that, device level simulations to understand these non-idealities, and exploration in the dynamic domain through *ac* measurements, also remain open for venturing into, in the future.

REFERENCES

[1] K.Hansen, "Wireless communications devices and technology: future directions," *IEEE Radio Frequency Integrated Circuits Symposium, Baltimore*, pp. 1–5, 1998.

[2] Technology Industry Association," *2005 Telecommunications Market Review and Forecast*, Available online at http://www.tiaonline.org/ media/mrf.

[3] J. D. Cressler and G. Niu, *Silicon Germanium Heterojunction Bipolar Transistors*, Artech House, Boston, 2002.

[4] J. D. Cressler et al., "On the Profile Design and Optimization of Epitaxial Si- and SiGe- Base Bipolar Technology for 77K Applications - Part I: Transistor DC Design Considerations," *IEEE Transactions on Electron Devices*, vol. 40, no. 3, March 1993

[5] A. J. Joseph et al., "Optimization of SiGe HBT's for Operation at High Current Densities," *IEEE Transactions on Electron Devices*, vol. 46, no. 7, July 1999.

[6] A. J. Joseph, "The Physics, optimization, and modeling of cryogenically operated SiGe HBTs, Ph.D Dissertation, Auburn University, 1997.

[7] H. Kroemer, "Heterostructure Bipolar Transistors and Integrated Circuits," *Proceedings of the IEEE*, vol. 70, no. 1, January 1982.

[8] A. Y. Cho and J. R. Arthur, "Molecular beam epitaxy," *Prog. Solid State Chem.*, vol. 10, pt. 3, pp. 157-191, Feb 1981.

[9] R. D. Dupuis et al., "Preparation and properties of $Ga_{1-x}Al_xAs$-GaAs heterojunctions grown by metal organic chemical vapor deposition," *Gallium Arsenide and Related Compounds 1978 (St. Louis), Inst. Phys. Conf. Ser.*, vol. 45, pp. 1-9, 1979.

[10] R. F. Pierret, *Semiconductor Device Fundamentals*, Addison-Wesley, Redding, 1996.

[11] S. S. Iyer et al., "Pseudomorphic growth of $Ge_xSi)1-x$ on silicon by molecular beam epitaxy," *Tech. Dig. IEEE Int. Elect. Dev. Meeting*, pp. 874-876, 1987.

[12] J. M. Matthews and A.E. Blakeslee, "Defects in epitaxial multilayers: I. misfit dislocations in layers," *J. Cryst. Growth*, vol. 27, pp. 118-125, 1974.

[13] J. M. Matthews and A.E. Blakeslee, "Defects in epitaxial multilayers: II. dislocation pileups, threading dislocations, slip lines, and cracks," *J. Cryst. Growth*, vol. 32, pp. 265-273, 1975.

[14] J. C. Bean et al., "Ge_xSi_{1-x}/Si Strained Layer Superlattice Grown by Molecular Beam Epitaxy," *Journal of Vacuum Science and Technology* , vol. A2, no. 2, pp. 436-440, 1984.

[15] S. R. Stiffler et al., "The Thermal Stability of SiGe Films Deposited by Ultrahigh-Vacuum Chemical Vapor Deposition," *Journal of Applied Physics*, vol. 70, no. 11, pp. 7194, 1991.

[16] G. L. Patton et al., "SiGe-Base Heterojunction Bipolar Transistor by Molecular Beam Epitaxy," *IEEE Electron Device Letters*, vol.9, no. 4. pp. 165-167, 1988.

[17] J. F. Gibbons et al., "Limited Reaction Processing: Silicon Epitaxy," *Applied Physics Letters*, Vol. 47, pp. 165-167, 1988.

[18] T. O. Sedgwick et al., " High Phosphorus Doping of Epitaxial Silicon at Low Temperature and Atmospheric Pressure," *Applied Physics Letters*, vol. 58, no. 14, pp. 1896-1898, 1991.

[19] B. S. Meyerson et al., "Low-Temperature Silicon Epitaxy by Ultrahigh Vacuum Chemical Vapor Deposition," *Applied Physics Letters*, vol. 48, no. 12, pp. 797-799, 1986.

[20] D.C. Ahlgren et al., "A SiGe HBT BiCMOS technology for mixed-signal RF applications," *Proc. IEEE Bipolar/BiCMOS Circ. Tech. Meeting* , pp. 195-198, 1997.

[21] A. Joseph et al., "A 0.18 μ"m BiCMOS technology featuring 120/100 GHz (f_T/f_{max}) HBT and ASIC compatible CMOS using copper interconect," *Proc. IEEE Bipolar/BiCMOS Circ. Tech. Meeting*, pp. 143-146, 2001.

[22] A. Joseph et al., "A 0.13 μ"m 210 GHz f_T SiGe HBTs - expanding the horizons of SiGe BiCMOS," *Tech. Dig. IEEE Int. Solid-State Circ. Conf.*, pp. 180-182, 2002.

[23] J.-S. Rieh, B. Jagannathan, H. Chen, K. T. Schonenberg, D. Angell, A. Chinthakindi, J. Florkey, F. Golan, D. Greenberg, S. J. Jeng, M. Khater, F. Pagette, C. Schnabel, P. Smith, A. Stricker, K. Vaed, R. Volant, D. Ahlgren, G. Freeman, K. Stein, and S. Subbanna, "SiGe HBTs with cut-off frequency of 350 GHz," *Technical Digest IEEE International Electron Devices Meeting*, pp. 771–774, Dec. 2002.

[24] J.-S. Rieh et al., "SiGe HBTs for Millimeter-Wave Applications with Simultaneously Optimized f_T and f_max of 300GHz," in *Technical Digest IEEE Radio Frequency Integrated Circuits Symposium*, pp. 395-398, 2004

[25] D.C. Ahlgren, G. Freeman, S. Subbanna, R. Groves, D. Greenberg, J. Malinowski, D. Nguyen-Ngoc, S.J. Heng, K. Stein, K. Schonenberg, D. Kiesling, B. Martin, S. Wu, D. Harame, and B. Meyerson, "A SiGe HBT BiCMOS technology for mixed-signal RF applications," *Proceedings of the Bipolar/BiCMOS Circuits and Technology Meeting*, pp. 195–197, 1997.

[26] A. Joseph, D. Coolbaugh, M. Zierak, R. Wuthrich, P. Geiss, Z. He, X. Liu, B. Orner, J. Johnson, G. Freeman, D. Ahlgren, B. Jagannathan, L. Lanzerotti, V. Ramachandran, J. Malinowski, H. Chen, J. Chu, P. Gray, R. Johnson, J. Dunn, S. Subbanna, K. Schonenberg, D. Harame, R. Groves, K. Watson, D. Jadus, M. Meghelli, and A.

Rylyakov, "A 0.18 μm BiCMOS technology featuring 120/100 GHz (f_T/f_{max}) HBT and ASIC-compatible CMOS using copper interconnect," *Proceedings of the IEEE Bipolar/BiCMOS Circuits and Technology Meeting*, pp. 143–146, 2001.

[27] E.O. Johnson, "Physical limitations on frequency and power parameters of transistors, " *RCA Review*, vol. 26, pp. 163-177, 1965.

[28] H. Kroemer, "Two integral relations pertaining to electron transport through a bipolar transistor with a nonuniform energy gap in the base region," *Solid-State Electronics*, vol. 28, pp. 1101–1103, 1985.

[29] E.J. Prinz, P.M. Garone, P.V. Schwartz, X. Xiao, and J.C. Sturm, "The effect of emitter-base spacers and strain-dependent density-of-states in Si/SiGe/Si heterojunction bipolar transistors," *Technical Digest IEEE International Electron Device Meeting*, pp. 639–642, 1989.

[30] D.L. Harame, J.H. Comfort, J.D. Cressler, E.F. Crabbe, J.Y-C. Sun, B.S. Meyerson, and T. Tice, "Si/SiGe epitaxial-base transistors – part I: materials, physics, and circuits," *IEEE Transactions on Electron Devices*, vol. 42, pp. 455–468, 1995.

[31] S.S. Iyer, G.L. Patton, J.M.C. Stork, B.S. Meyerson, and D.L. Harame, "Heterojunction bipolar transistors using Si-Ge alloys," *IEEE Transactions on Electron Device*, vol. 36, pp. 2043–2064, 1989.

[32] E. F. Crabble et al., "Current Gain Rolloff in Graded-Base SiGe Heterojunction Bipolar Transistors," *IEEE Electron Device Letters*, vol. 14, no. 4, April 1993.

[33] J. D. Cressler et al., "An Epitaxial Emitter-Cap SiGe-Base Bipolar Technology Optimized for Liquid-Nitrogen Temperature Operation," *IEEE Electron Device Letters*, vol. 15, no. 11, November 1994.

[34] A. J. Joseph et al., "Optimization of SiGe HBT's for Operation at High Current Densities," *IEEE Transactions on Electron Devices*, vol. 46, no. 7, July 1999.

[35] G. Niu, J. D. Cressler, S. Zhang, U. Gogineni, and D. C. Ahlgren, "Measurement of collector-base junction avalanche multiplication effects in advanced UHV/CVD SiGe HBT's," *IEEE Transactions on Electron Devices*, vol. 46, pp. 1007–1015, 1999.

[36] J. D. Hayden, D. Burnett, J. Nangle, "A comparison of base current reversal and bipolar snapback in advanced n-p-n bipolar transistors," *IEEE Electron Device Letters*, vol 12, pp. 407–409, 1991.

[37] M. R. Shaheed and C. M. Maziar, "Extension of common-emitter breakdown voltage for high speed Si/SiGe HBT's," *IEEE Bipolar Circuits and Technology Meeting*, pp. 42–45, 1992.

[38] J. S. Yuan, "Base current reversal in bipolar transistors and circuits: a review and update," *Circuits, Devices, and Systems, IEE Proceedings*, vol. 141, pp. 299–306, 1994.

[39] P. F. Lu and C. T. Chuang, "Effect of reverse base current on bipolar and BiCMOS circuits," *IEEE Transactions on Electron Devices*, vol. 39, pp. 1902–1908, 1992.

[40] P. F. Lu and T. C. Chen, "Collector-Base junction avalanche effects in advanced double-poly self-aligned bipolar transistors," *IEEE Transactions on Electron Devices*, vol. 36, pp. 1182–1188, 1989.

[41] J. S. Rieh, B. Jagannathan, D. Greenberg, G. Freeman, and S. Subbanna, "A doping concentration-dependent upper limit of the breakdown voltage-cutoff frequency product in Si bipolar transistors," *Solid State Electronics*, vol. 48, pp. 339–343, 2003.

[42] S. Tiwari, "A new effect at high currents i heterostructure bipolar transistors," *IEEE Elect. Dev. Lett.*, vol. 9, pp. 142-144, 1988.

[43] A. J. Joseph et al., "Impact of profile scaling on high-injection barrier effects in advanced UHV/CVD SiGe HBTs," *Tech. Dig. IEEE Int. Elect. Dev. Meeting*, pp. 253-256, 1996.

[44] B. Banerjee, et al., "Cryogenic Operation of Third-Generation, 200 GHz Peak-f_T, Silicon-Germanium Heterejunction Bipolar Transistors, *IEEE Transactions on Electron Devices*, vol. 52, no. 4, April 2005

[45] Q. Liang, R. Krithivasan, A. Ahmed, Y. Lu, Y. Li, J. D. Cressler, G. Niu, J.-S. Rieh, G. Freeman, D. Ahlgren, and A. Joseph, "Analysis and Understanding of Unique Cryogenic Phenomena in State-of-the-art SiGe HBTs,"*IEEE Transactions on Electron Devices*, vol. 37, pp. 2151–2156, 2002.

[46] G. Freeman, J. S. Rieh, B. Jagannathan, Y. Zhijian, F. Guarin, A. Joseph, and D. Ahlgren, "SiGe HBT performance and reliability trends through f_T of 350GHz," *Proceedings of the IEEE International Reliability Physics Symposium*, pp. 332–338, 2003.

[47] J. D. Cressler, "Emerging SiGe HBT reliability issues for mixed-signal circuit applications," *IEEE Transactions on Device and Materials Reliability*, vol. 4, pp. 222–236, 2004.

[48] G. Zhang, J. D. Cressler, G. Niu, and A. J. Joseph, "A new "mixed-mode" reliability degradation mechanism in advanced Si and SiGe bipolar transistors," *IEEE Transactions on Electron Devices*, vol. 37, pp. 2151–2156, 2002.

[49] C. Zhu, Q. Liang, R. Al-Huq, J. D. Cressler, A. J. Joseph, J. Johansen, T. Chen, G. Niu, G. Freeman, J. S. Rieh, D. Ahlgren, "An investigation of the damage mechanisms in impact ionization-induced "mixed-mode" reliability stressing of scaled SiGe HBTs," *Technical Digest IEEE International Electron Devices Meeting*, pp. 185–188, 2003.

[50] J.-S. Rieh, B. Jagannathan, H. Chen, K. T. Schonenberg, D. Angell, A. Chinthakindi, J. Florkey, F. Golan, D. Greenberg, S. J. Jeng, M. Khater, F. Pagette, C. Schnabel,

P. Smith, A. Stricker, K. Vaed, R. Volant, D. Ahlgren, G. Freeman, K. Stein, and S. Subbanna, "SiGe HBTs with cut-off frequency of 350 GHz," *Technical Digest IEEE International Electron Devices Meeting*, pp. 771–774, Dec. 2002.